remote sensing

MDPI

Article

Comparison of Aerosol Optical Depth from MODIS Product Collection 6.1 and AERONET in the Western United States

Iyasu G. Eibedingil [1,*], Thomas E. Gill [1,2], R. Scott Van Pelt [3] and Daniel Q. Tong [4]

1 Environmental Science and Engineering Program, University of Texas at El Paso, El Paso, TX 79968, USA; tegill@utep.edu
2 Department of Earth, Environmental and Resource Sciences, University of Texas at El Paso, El Paso, TX 79968, USA
3 USDA–Agricultural Research Service, Big Spring, TX 79720, USA; scott.vanpelt@usda.gov
4 Department of Atmospheric, Ocean and Earth Sciences, George Mason University, Fairfax, VA 22030, USA; qtong@gmu.edu
* Correspondence: igeibedingil@miners.utep.edu

Abstract: Recent observations reveal that dust storms are increasing in the western USA, posing imminent risks to public health, safety, and the economy. Much of the observational evidence has been obtained from ground-based platforms and the visual interpretation of satellite imagery from limited regions. Comprehensive satellite-based observations of long-term aerosol records are still lacking. In an effort to develop such a satellite aerosol dataset, we compared and evaluated the Aerosol Optical Depth (AOD) from Deep Blue (DB) and Dark Target (DT) product collection 6.1 with the Aerosol Robotic Network (AERONET) program in the western USA. We examined the seasonal and monthly average number of Moderate Resolution Imaging Spectroradiometer (MODIS) Aqua DB AOD retrievals per $0.1^\circ \times 0.1^\circ$ from January 2003 to December 2017 across the region's different topographic, climatic, and land cover conditions. The number of retrievals in the southwest United States was on average greater than 37 days per 90 days for all seasons except summer. Springtime saw the highest number of AOD retrievals across the southwest, consistent with the peak season for synoptic-scale dust events. The majority of Arizona, New Mexico, and western Texas showed the lowest number of retrievals during the monsoon season. The majority of collocating domains of AOD from the Aqua sensor showed a better correlation with AERONET AOD than AOD from Terra, and the correlation coefficients exhibited large regional variability across the study area. The correlation coefficient between the couplings Aqua DB AOD-AERONET AOD and Terra DB AOD-AERONET AOD ranges from 0.1 to 0.94 and 0.001 to 0.94, respectively. In the majority of the sites that exhibited less than a 0.6 correlation coefficient and few matched data points at the nearest single pixel, the correlations gradually improved when the spatial domain increased to a 50 km × 50 km box averaging domain. In general, the majority of the stations revealed significant correlation between MODIS and AERONET AOD at all spatiotemporal aggregating domains, although MODIS generally overestimated AOD compared to AERONET. However, the correlation coefficient in the southwest United States was the lowest and in stations from a higher latitude was the highest. The difference in the brightness of the land surface and the latitudinal differences in the aerosol inputs from the forest fires and solar zenith angles are some of the factors that manifested the latitudinal correlation differences.

Keywords: aerosols; MODIS; AERONET; deep blue; dark target; Angstrom exponent

check for updates

Citation: Eibedingil, I.G.; Gill, T.E.; Van Pelt, R.S.; Tong, D.Q. Comparison of Aerosol Optical Depth from MODIS Product Collection 6.1 and AERONET in the Western United States. *Remote Sens.* **2021**, *13*, 2316. https://doi.org/10.3390/rs13122316

Academic Editor: Michaël Sicard

Received: 13 May 2021
Accepted: 10 June 2021
Published: 13 June 2021

Publisher's Note: MDPI stays neutral with regard to jurisdictional claims in published maps and institutional affiliations.

Copyright: © 2021 by the authors. Licensee MDPI, Basel, Switzerland. This article is an open access article distributed under the terms and conditions of the Creative Commons Attribution (CC BY) license (https://creativecommons.org/licenses/by/4.0/).

1. Introduction

Aerosols affect the climate system through direct radiative forcing [1,2], indirect radiative forcing [3], and modulation of heterogenous chemistry [4]. They adversely impact human health [5,6], the environment [7,8], and the economy [9]. Linked to its major deserts in the southwest and highly vegetated mountainous ecoprovinces, the western United

States is a source of many types of aerosols including both direct and chemically transformed emissions injected from natural and anthropogenic sources (e.g., dust, biomass burning, power plants, biogenic aerosols, and mobile source emissions) [10,11]. Considerable evidence indicates that during the past few decades the western United States has been experiencing an increase in the frequency and intensity of dust events and wildfires; the dust dominated aerosols mainly originate from the deserts and plains, and wildfire aerosols from forest, woodland, and grassland ecoprovinces. Tong et al. [12] reported a rapid intensification of dust storm activity over American deserts in the time range 1988–2011. Brahney et al. [13] revealed that the American West is becoming increasingly dusty based on the Ca^{+2} composition of precipitation from 1994 to 2009. Using iron as a proxy of mineral dust, Hand et al. [14] showed an increasing trend of dust in large parts of the western United States with +5% per year change from 1995 to 2015 during the normally dusty month of March, an effective doubling of March dust concentration during the two decades. Wildfires have also been contributing to large amounts of aerosols into the atmosphere over the American West [15–18]. McClure & Jaffe [18] showed that since the mid 1980s, the total area of the United States that has been burned by wildfires has been increasing with fires in the northwest United States accounting for around 50-60% of that increase. Climate change and variability in different climate parameters significantly contributes to the increase in wildfires [19]. Littell et al. [16] documented that most of the vegetation zones in the western United States exhibited strong year-of-fire relationships with low precipitation, intense drought, and high temperature.

In recent decades, aerosol products from satellite remote sensing, ground-based observations, and models have been widely synthesized to monitor the temporal and spatial distribution of aerosol loading on global and regional scales [20–25]. Remote sensing imagery products from the Moderate Resolution Imaging Spectroradiometer (MODIS) sensor aboard the Aqua and Terra satellites provide retrieved data on aerosol properties at a near-daily global coverage and a wide range of spatial and spectral resolutions. However, due to the potential influences of retrieval algorithms, surface albedo, topography, shadow, and image resolutions, the satellite products should be continuously validated to minimize the uncertainties [26–28]. Aerosol data acquired from ground stations, more specifically ground-based remote sensing approaches such as the Aerosol Robotic Network (AERONET), are crucial resources in ground-truthing satellite products as they have a higher precision of measurement at a low spatial reach [29]. The AERONET is a direct columnar measurement acquired by sunphotometer and aggregated in time at the point location. However, the satellite Aerosol Optical Depth (AOD) is a columnar measurement retrieved through radiative-transfer models based on multiple assumptions about aerosols and surface characteristics leading to various sources of uncertainty [30,31]. Satellite AOD (including MODIS) represents the AOD concentration for a fraction of a minute when a satellite is on orbit over a region [32].

Several researchers have investigated the relationship between satellite remote-sensed and ground-based aerosol products by collating both data products to characterize aerosol loading to the atmosphere in space and time [33–36]. Bréon et al. [33] evaluated the accuracy of aerosol products retrieved from the measurements of multiple satellite remote sensing instruments by comparing with AOD from the AERONET program on a global scale. Saide et al. [35] examined the performance of the aerosol data matrix from the assimilation of AOD retrieval from Geostationary Ocean Color Imager (GOCI) and MODIS instruments by comparing against the ground measurement of AERONET AOD and PM_{10} in northeast Asia. Vijayakumar et al. [36] investigated dust-dominated aerosol characteristics during a specific dust event in western India by augmenting aerosol data from MODIS and AERONET, and with meteorological data of model simulations from the European Center for Medium-Range Weather Forecasts Reanalysis-Interim (ERA-Interim). Similarly, many studies utilized satellite, model simulations, and ground-based data to improve air quality modeling and forecasting in the United States [37–40], mainly focusing on the eastern United States. For example, Li et al. [39] used AOD data processed from

MODIS, Multi-angle Imaging SpectroRadiometer (MISR), Sea-viewing Wide Field-of-view Sensor (SeaWiFS), and Ozone Monitoring Instrument (OMI) image products and the results were verified against AERONET AOD measurements.

Although air quality in the western United States has improved during the past few decades [41], different studies have revealed that air pollution has increased nationally since 2016 [42]. For example, according to a report from the United States Environmental Protection Agency [43], the southwest has experienced an abrupt increase of PM_{10} pollution from 2015 primarily linked to mineral aerosol loading and the northwest showed a spike in $PM_{2.5}$ pollution contributed by wildfires. In addition, Tong et al. [12] documented that in the American deserts, the frequency of windblown dust storms has increased by 240% from the 1990s to the 2000s. In an effort to develop a more comprehensive and long-term fusion of ground-based and satellite-based observations, and to facilitate the validation of satellite remote sensing imagery products, this study compares and evaluates the AOD from MODIS Deep Blue (DB) and Dark Target (DT) product collection 6.1 with AERONET AOD in the western United States bounded by the -92° meridian in the east.

2. Study Area

The study area encompasses the western part of the United States bounded by the -92° meridian in the east, including parts of 22 states (Figure 1). This region is a land of extremes. It contains several major ecological regions (Figure 1a): Warm and cold deserts, coastal and inland forests, coastal and alpine environments, shrublands and grasslands, distributed from -105 to 4302 m elevation (Figure 1b). Mainly influenced by differences in elevation and the climatological influence of the Pacific Ocean, the climate of the western United States is very diverse in nature [44]. Due to this variation, the region is subjected to a diverse spectrum of natural and anthropogenic aerosols and impacts. The black (Figure 1a) and blue (Figure 1b) dots show the AERONET stations over the western United States, located in a wide range of ecological regions and elevations. Depending on their proximity to different ecosystems and land uses, these stations can be exposed to different aerosol sizes and types.

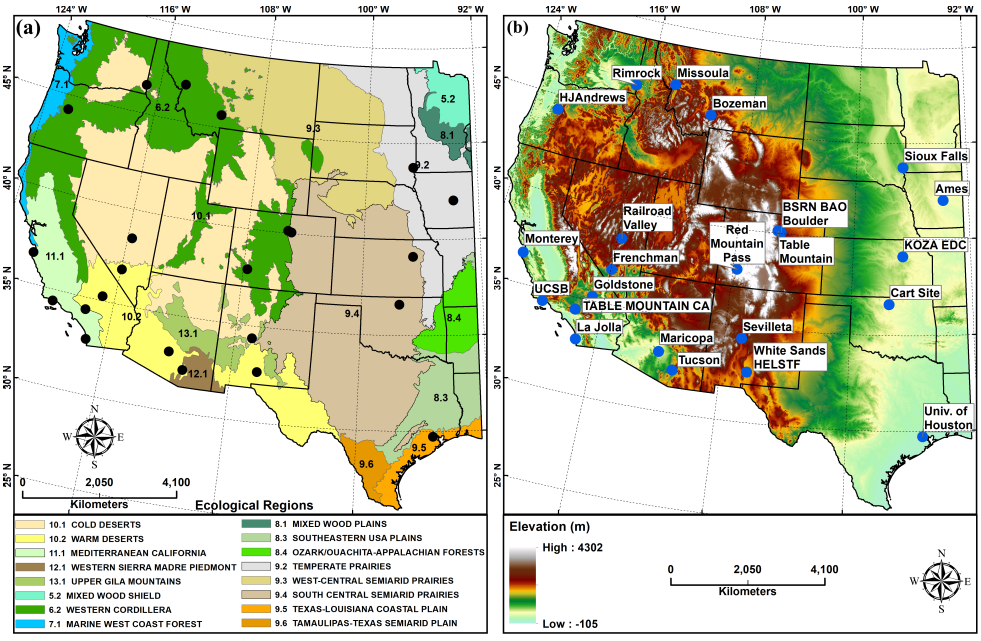


Figure 1. (**a**) Ecological regions of the western United States acquired from the Commission for Environmental Cooperation (US Environmental Protection Agency). Black dots represent the AERONET stations. (**b**) Digital Elevation Model (DEM) map of the western United States extracted from global GTOPO30 model at 30 arc seconds (≈1 km) spatial resolution (USGS). Black and blue dots represent the AERONET stations.

3. Data

3.1. AERONET

The ground-based data used for this study were acquired from the AERONET network program. AERONET is a federated instrument network of sunphotometers and data archive for aerosol characterization under the administration of the NASA Goddard Space Flight Center [45]. The AERONET program uses sunphotometers that measure direct solar irradiance and sky radiance at the Earth's surface [46]. The sunphotometers are directed at the sun (or the moon if the sensitivity is high enough) and the output delivers a direct measurement of the extinction of light between the top of the atmosphere and the Earth's surface, which is directly related to AOD. In addition, using this measurement enabled other columnar optically effective aerosol properties to be acquired including volume size distribution, complex index of refraction, Angstrom exponent, and single scattering albedo. The spatial representation of AERONET sites vary between a 200- and 500-km radius depending on the specific locations influenced by topographic and climatic conditions [47]. The measurement is acquired every 15 min at eight spectral bands (340, 380, 440, 500, 675, 870, and 1020 nm). Three versions of data are available for three data quality levels: Level 1.0 (unscreened), Level 1.5 (cloud-screened and quality controlled), and Level 2 (quality assured).

We used Level 2 data of 23 AERONET stations (Figure 1 and Table 1) over the western United States. These sites were selected for analysis based on the availability of more than five years of data record and the geographic location west of 90° west longitude. Since AERONET AOD data were not available at a 550-nm wavelength, equivalent AERONET AOD at 550 nm ($\tau_{550\text{nm}}$) values were determined by interpolating AERONET AODs reported at 500 and 675 nm spectral channels and Angstrom exponents at 440–675 nm ($\alpha_{440-675}$) using the Angstrom exponent formula in (Equation (1)) [48,49].

$$\tau_{550\text{nm}} = \frac{\tau_{500\text{nm}}}{exp(-\alpha * ln(\frac{\lambda_{500\text{nm}}}{\lambda_{550\text{nm}}}))} \quad (1)$$

where $\tau_{550\text{nm}}$ and $\tau_{500\text{nm}}$ are AOD at wavelengths 550 ($\lambda_{550\text{nm}}$) and 500 ($\lambda_{500\text{nm}}$) nm, respectively. This processing was applied to all 23 sites.

3.2. MODIS

MODIS sensors aboard NASA's Aqua and Terra satellites acquire near-global daily measurements using 36 spectral bands in a wide spectral range (410 to 1500 nm) [30]. MODIS on the Aqua platform was launched in December 1999 and on the Terra platform in late May 2002 [50]. Retrieved from the calibrated radiance/reflectance measurements, the MODIS Level 2 aerosol products (MYD04 from Aqua and MOD04 from Terra) monitor the ambient columnar aerosol loading and other aerosol properties over cloud-free and snow/ice-free land and ocean surfaces. Aerosol products for land are retrieved using Deep Blue (DB) and Dark Target (DT) algorithms at a nominal spatial resolution of 10 km × 10 km at nadir. These algorithms synthesize different assumptions about the Earth's surface and the expected aerosol types above these surfaces [51]. The standard aerosol product from Dark Target method works best over dark vegetated regions and does not work well over bright land surfaces. Extraction of aerosol properties from satellite imagery over bright surfaces (such as prevalent in arid and semiarid lands) is a challenging issue at many wavelengths of visible light. The DB algorithm is powerful in retrieving aerosol products over bright desert surfaces because it utilizes two blue channels (412 and 470 nm) to discern the reflectance between the land surface and aerosols [52–54], but it can also retrieve over highly vegetated targets. In these channels, aerosols tend to be bright and land surface features dark. The DB algorithm reports AOD at 550, 412, 470, and 670 nm, Angstrom exponent at 412–470 nm, and single scattering albedo at 412, 470, and 670 nm.

Table 1. Geographic information, time range of available data at AERONET sites [45], and land cover/land use type (https://nationalmap.gov/small_scale/mld/landcvi.html (accessed on 1 October 2019) for 23 sites.

Site ID	Site Name	State	Coordinates		Elevation (m)	Period of Record		LULC Type
			Long.	Lat.		Start	End	
St. 1	Ames	IA	−93.775	42.021	338.0	20040521	20160102	Rural, dryland cropland, and pasture
St. 2	Bozeman	MT	−111.045	45.662	1507.0	20080411	20170419	Urban, shrubland, and grassland
St. 3	BSRN BAO Boulder	CO	−105.006	40.045	1604.0	20010507	20160713	Urban and cropland/grassland mosaic
St. 4	CART Site	OK	−97.486	36.607	318.0	19940407	20170623	Rural, dryland cropland, and pasture
St. 5	Frenchman Flat	NV	−115.935	36.809	940.0	20061212	20150126	Rural and shrubland
St. 6	Goldstone	CA	−116.792	35.233	1100.0	20091216	20170816	Rural and shrubland
St. 7	HJAndrews	OR	−122.224	44.239	830.0	19950622	20111221	Evergreen Needleleaf Forest
St. 8	Konza EDC	KS	−96.610	39.102	341.0	20000616	20151203	Rural and cropland/grassland mosaic
St. 9	La Jolla	CA	−117.251	32.868	80.0	20000229	20131021	Urban, ocean, grassland, and builtup land
St. 10	Maricopa	AZ	−111.972	33.069	360.0	20000324	20100709	Rural and shrubland
St. 11	Missoula	MT	−114.083	46.917	976.0	20000824	20170815	Urban, grassland, and needleleaf forest
St. 12	Monterey	CA	−121.855	36.593	50.0	19980513	20161004	Urban, built-up land, and needleleaf forest
St. 13	Railroad Valley	NV	−115.691	38.497	1437.0	20110626	20150825	Rural, barren, and mixed shrubland/grassland
St. 14	Red Mountain Pass	CO	−107.711	37.907	3376.0	20051005	20170928	Rural and mixed forest
St. 15	Rimrock	ID	−116.992	46.487	824.0	19990414	20170316	Grassland, dryland cropland, and pasture
St. 16	Sevilleta	NM	−106.885	34.355	1477.0	19940411	20170423	Rural and shrubland
St. 17	Sioux Falls	SD	−96.626	43.736	505.0	19970718	20171024	Rural, dryland cropland, and pasture
St. 18	Table Mountain	CO	−105.237	40.125	1689.0	19980805	20171228	Grassland
St. 19	Table Mountain CA	CA	−117.680	34.380	2200.0	19980805	20171228	Evergreen needleleaf forest
St. 20	Tucson	AZ	−110.953	32.233	779.0	19931119	20161122	Urban and built-up land
St. 21	UCSB	CA	−119.845	34.415	33.0	20021208	20170917	Urban, ocean, grassland, and built-up land
St. 22	Univ. of Houston	TX	−95.342	29.718	65.0	20060820	20160902	Urban, ocean, and built-up land
St. 23	White Sands HELSTF	NM	−106.338	32.635	1207.2	20061117	20170626	Rural, shrubland, and barren

In the present study, we used the latest Deep Blue Level 2 MODIS aerosol products collection 6.1 from Aqua and Terra satellites, MYD04_L2 and MOD04_L2, respectively. The uncertainty of the retrieved Terra MODIS DB AOD collection 6.1 is $0.03 \pm 21\%$ and $0.03 \pm 18\%$ with respect to the ground-truth measurement of AERONET AOD ($0.03 \pm 0.21 \times$ AODAERONET and $0.03 \pm 0.18 \times$ AODAERONET) for arid and vegetated path retrievals, respectively [55]. Thus, collection 6.1 has a slightly better performance than collection 6.0. The DB aerosol product in collection 6.1 is generated by an Enhanced DB algorithm [54] by improving collection 6.0. The improvements include heavy smoke detection, artefact reduction over heterogenous terrain, improved surface modeling for elevated terrain, and bug fixes and updated regional/seasonal aerosol optical models [56]. The MYD04_L2 and MOD04_L2 data products were ordered and downloaded from the Atmosphere Archive and Distribution System (LAADS) Distributed Active Archive Center (DAAC) website (https://ladsweb.modaps.eosdis.nasa.gov (accessed on 1 June 2018)) covering the western United States from July 2002 to June 2018. We used daily Deep Blue AOD at 550 nm and Angstrom exponent for land at a 10 km $\times$ 10 km spatial resolution with all the available quality flags. The DB AOD is represented by the data field name "Deep_Blue_Aerosol_Optical_Depth_550_Land". The DT AOD is represented by the field name "Optical_Depth_Land_And_Ocean" which is aerosol optical thickness at 550 nm for both ocean (best) and land (corrected). The interpolation of AERONET and MODIS AOD, the extraction of MODIS AOD for the AERONET coordinate locations, and the statistical analysis were batch processed using MATLAB and Python software packages.

4. Methods

4.1. Assessment of the Number of Pixels of MODIS DB AOD Retrieval

We investigated the long-term monthly and seasonal average distribution of MODIS Aqua DB AOD retrieval per the interpolation grid cell per season and month averaged from 2003 to 2017 for the western United States. This analysis can give us information about the applicability of the aerosol product in different regions, frequency of days impacted by poor air quality associated with aerosols, and impact of cloud and snow on the number of retrievals. For this analysis we used the interpolated images created from the Level 2 granules overlapping the study area. This methodology was applied to facilitate the assessment by utilizing images with regular latitude and longitude grids rather than on irregularly spaced pixels along the orbit track (Level 2) [57]. This is performed by linearly interpolating the Level 2 granules from each day using an interpolation function from MATLAB. All pixels covering the study area were arranged into one daily file. Then, linear interpolation was applied at every fixed matrix point ($0.1^\circ \times 0.1^\circ$) weighing the surrounding Level 2 values by the fraction of overlapping area between the two grids. As a result, a total of 5786 files were produced extending from 4 July 2002 to 22 May 2018. Aqua products were used based on the higher correlation with AERONET AOD, discerned during the research process.

4.2. Comparison of MODIS and AERONET AOD

Aerosol optical depth retrieved from MODIS DB and DT product collection 6.1 were compared with AOD data from 23 AERONET sites. We also investigated the correlation of AOD between the couplings of MODIS Aqua–AERONET and MODIS Terra–AERONET. For this analysis, we used the original (irregular grid) Level 2 product with the data field name "Deep_Blue_Aerosol_Optical_Depth_550_Land" from both Aqua (MYD04_L2) and Terra satellites (MOD04_L2). The time series of MODIS AOD were extracted for the AERONET station locations by considering different combinations of temporal and spatial domains.

Spatially, we considered three different scenarios. The MODIS AOD pixels nearest to the AERONET sites were identified using the Euclidean distance method. The determined pixels were denoted as single pixels or a centroid representing AERONET sites, by limiting the distance between the center of pixels to a radius $\leq$ 10 km. In addition, we examined the

impact of regions surrounding the centroids by considering two different spatial averaging domains of AOD values, the nearest nine and twenty-five pixels. For the nine pixels scenario (30 km × 30 km box or 3 × 3 pixels), AOD from the identified central points and its nearest eight surrounding pixels were averaged by setting the threshold radius distance of 20 km or less. Similarly, for the 25-pixel scenario (50 km × 50 km box or 5 × 5 pixels), AOD from the identified central points and its nearest 24 pixels were averaged by limiting the radius distance to 30 km or less.

Likewise, we considered three averaging temporal domains, nearest data, 30-min and 3-h averaging domains. The closest single MODIS AOD to the AERONET AOD were identified by limiting the difference to less than or equal to 10 min, otherwise the data were not included in the correlation analysis. For the 30-min and 3-h averaging domains, all of those AERONET AOD measurements within ±15 min and ±90 min of the MODIS overpass time were aggregated. These three temporal scenarios were applied to the AERONET AOD corresponding to the MODIS AOD retrievals averaged at the nearest single pixel and within 30 km × 30 km and 50 km × 50 km boxes. Using the mean as a statistical measure of central tendency is appropriate as it saves the mode of the quality flags from each pixel within the averaging domain [58]. After running the correlation analysis between all the corresponding collocated MODIS DB AOD and AERONET AOD measurements at all spatiotemporal scenarios, the results were compared with the correlation between MODIS Dark Target (DT) AOD and AERONET AOD at similar spatiotemporal settings. Here, we used the scientific data set named "Optical_Depth_Land_And_Ocean" at 550 nm from the Dark Target (DT) algorithm with all quality assurance flags.

5. Results

5.1. Assessment of the Number of Pixels of MODIS DB AOD Retrievals

The long term seasonal and monthly average numbers of MODIS DB AOD retrievals per 0.1° × 0.1° grid averaged from January 2003 to December 2017 are presented in Figure 2 and 3, respectively. The results revealed that the southwestern United States showed a significant number of retrievals per long-term average seasonal and monthly distribution during the same period. During the summer months (June, July, and August) the majority of Arizona, New Mexico, and western Texas, which experience a wet monsoon during that time, showed the lowest number of AOD retrievals. As the climate is very dry, the number of retrievals in the southwestern United States was on average greater than 14.8 days (≈50%) per 30 days for the majority of months and more than 37 days (≈41%) per 90 days for the three seasons other than June, July, and August. On the other hand, the states of California and Oregon exhibited the highest retrieval during summer reaching from 65 to 85 days per 90 days. During winter (December, January, and February), the northern part of the study area experienced either no or the lowest number of retrievals due to the presence of snow and cloud cover. Due to their high reflectivity, snow and clouds interfere with the AOD retrieval by making the separation of the radiance contribution from the surface and aerosols very difficult. In addition, some regions did not show any retrieval possibly due to the exclusion of pixels due to the contribution of reflectance from water bodies.

5.2. Evaluation of MODIS AOD Using AERONET AOD

We evaluated the robustness of the MODIS AOD product against the in-situ records of AERONET AOD. To validate the respective MODIS DB (land) and DT (land and ocean) AOD from Aqua and Terra satellites against a ground-based AERONET AOD, we fitted a linear regression model at all spatiotemporal scales. After running the model, we also extracted the Pearson correlation coefficient (R), *p*-value (P), number of samples (N), and root mean square error (RMSE) to measure the performance of the fitted models. Spatially, we considered the nearest single pixel to the AERONET station, 3 pixels by 3 pixels (corresponding to 30 km × 30 km), and 5 pixels by 5 pixels box (corresponding to 50 km × 50 km) as aggregating domains of MODIS AOD retrievals using the AERONET locations as the

center of the boxes. Temporally, we used the nearest single record to the MODIS AOD, 30 min (15 min before and after) and 3 h (90 min before and after) for averaging AERONET AOD using the MODIS AOD as a center time.

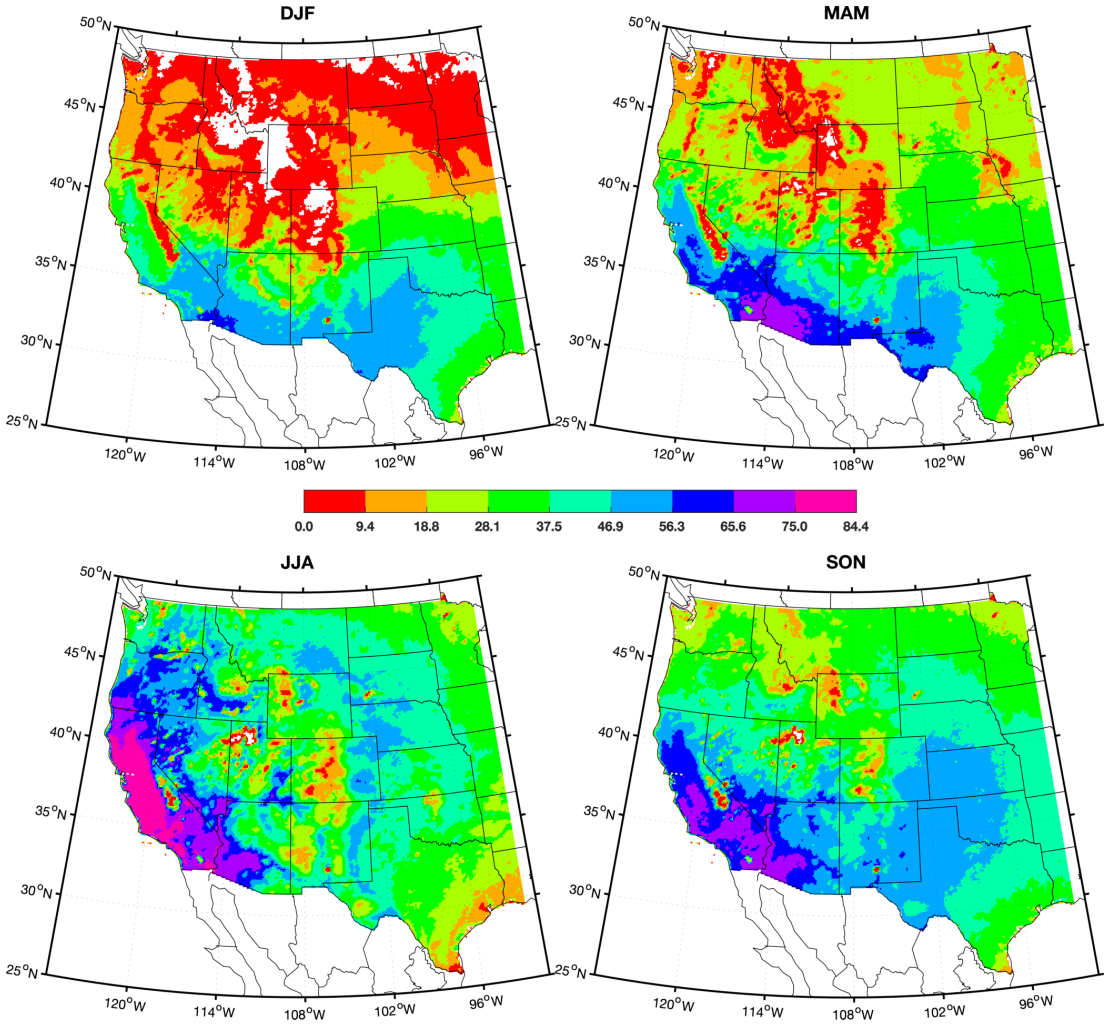


Figure 2. Seasonal distribution of the number of MODIS DB AOD retrieval per 0.1° × 0.1° averaged from January 2003 to December 2018.

The results for correlation analysis between MODIS (Aqua and Terra) DB AOD and AERONET AOD at different spatiotemporal scenarios are presented in Figure 4–6, and Table A1. The findings revealed strong and statistically significant (p-value < 0.05) correlation between MODIS DB and AERONET AOD at all spatial and temporal scales in the majority of stations, except the Red Mountain Pass station which showed a very weak and insignificant correlation at limited spatiotemporal scenarios. This is mainly linked to high cloud and snow cover in the high altitude area of the Rocky Mountains (Figure 5 and Table A1). The Pearson correlation coefficient between the couplings Aqua AOD–AERONET AOD and Terra AOD–AERONET AOD ranges from 0.1 to 0.94 and 0.001 to 0.94, respectively, with 19 stations scoring greater than 0.4 as the correlation coefficient. The Missoula station exhibited the strongest correlation (Figure 6) and the Red Mountain Pass the weakest correlation at all averaging domains. Overall, at the majority of collocating domains AOD from Aqua sensor showed a better correlation with AERONET AOD as compared to that of AOD from Terra. Therefore, in this region, Aqua AOD in combination with ground-based AOD and fine particulate matter measurements may be a better choice for air quality assessment, unless there is a diurnal component to the AOD-PM relationship influenced by changes in the boundary layer, or changes in relative humidity, etc. For ex-

ample, a combination of these data can be employed for estimating the ground-level fine particulate matter from columnar aerosol loading using different statistical approaches including machine learning and deep learning methods.

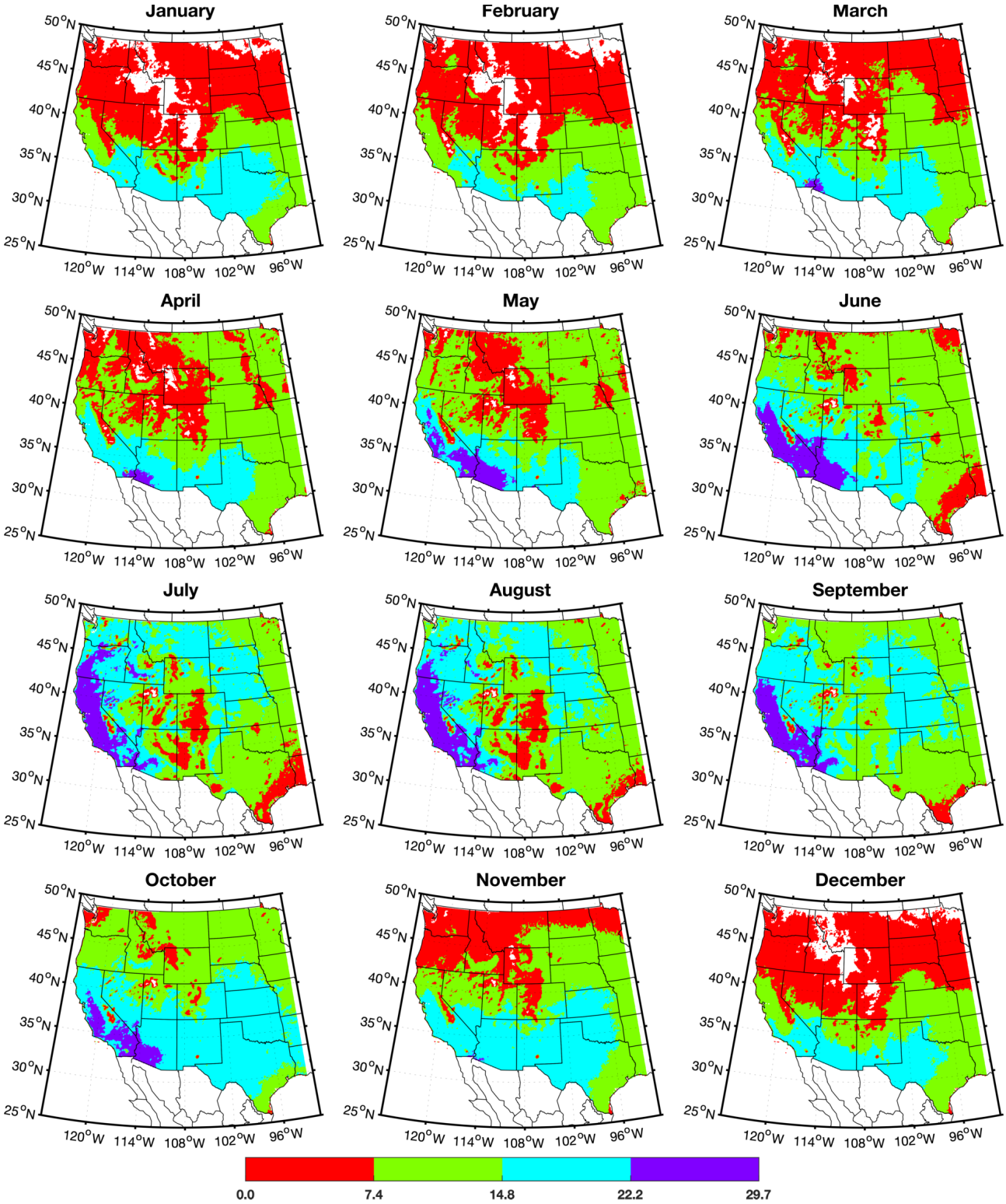


Figure 3. Long-term mean monthly distribution of the number of MODIS DB AOD retrieval per 0.1° × 0.1° averaged from January 2003 to December 2017.

The relationship between Aqua MODIS DB AOD and AERONET AOD showed a combination of decreasing and increasing correlation with the increase in spatiotemporal averaging domains (Figure 4 and 5). The stations that showed a strong correlation (greater than 0.6 except the University of Houston and Rimrock sites) and a slight increase in the number of matched samples, experienced a gradual decrease in the correlation coefficient with an increase in the spatial domain from the nearest single pixel to 50 km × 50 km aggregating domain. The University of Houston and Rimrock sites showed very similar concentrations in the immediate and up-to-50-km radius region. However, in the majority of the sites that exhibited less than a 0.6 correlation coefficient and very few matched data points at the nearest single pixel, the correlations gradually improved when the spatial domain increased to the 50 km × 50 km box averaging domain (Figure 5). The correlation analysis between Terra DB AOD and AERONET AOD showed a similar pattern to the Aqua DB AOD–AERONET couplings at all stations, except at CART Site, Monterey, Sevilleta, Sioux Falls, and Table Mountain stations that reversed the correlation trend by changing from the lowest to highest spatial domains. This reversal could be mainly due to the changes on the availability of matched AOD measurements linked to the overpass time of Aqua and Terra satellites, as the overpass time affects the number of matched samples.

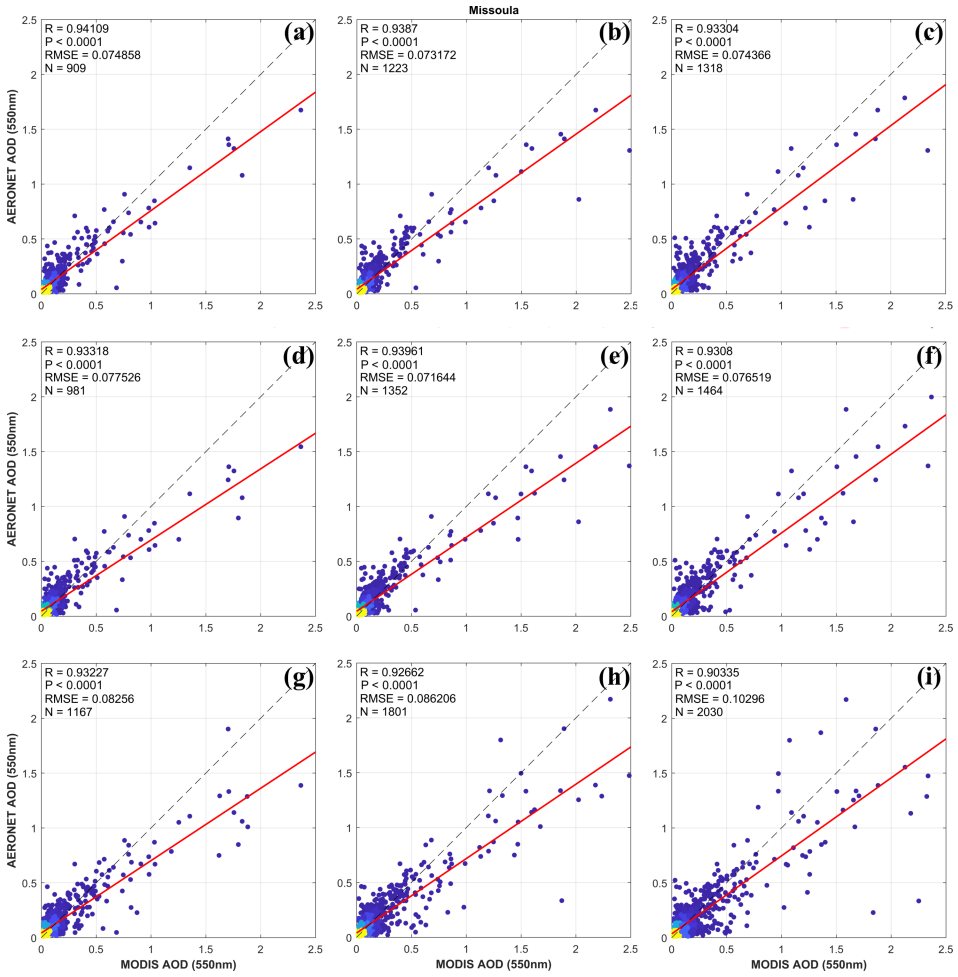


Figure 4. Scatter plots representing the validation of Aqua MODIS DB AOD against AERONET AOD processed at 550 nm of the representative Missoula station: Nearest single pixel in time (**a**) nearest singel pixel in space, averaged from nearest (**b**) 9 pixels, and (**c**) 25 pixels; 30 min averaging domain (**d**) nearest single pixel in time, averaged from nearest (**e**) 9 pixels, and (**f**) 25 pixels; and 3-h averaging domain (**g**) nearest single pixel in time, averaged from nearest (**h**) 9 pixels, and (**i**) 25 pixels. The red line is a regression line. Where R—Pearson correlation coefficient, P—*p* value, RMSE—root mean square error at 5% significance level, and N—number of matched AOD points. The one-to-one agreement is represented by the dashed line.

When the temporal collocation of AERONET AOD to the nearest ±15 min and ±90 min of Aqua and Terra MODIS overpass time was performed, the relationship was changed in terms of correlation coefficient, *p* value, and number of samples (Figure 5 and Table A1). From this analysis, the correlation between Aqua MODIS DB AOD from the nearest pixel and AERONET AOD increased at 14 stations (representing a wide range of ecoregions), when the temporal scenario of AERONET AOD increased from the nearest single pixel to ±15 min (Figure 5). A total of 11 of these 14 stations then exhibited a drop in correlation when the temporal aggregating domain increased from ±15 to ±90 min. However, the other nine stations showed a decreasing correlation trend from the nearest single pixel to ±15 min averaging extent (Figure 5). Five out of the nine stations then further showed a decrease in correlation when the AERONET AOD averaged increased to ±90 min of Aqua MODIS overpass time.

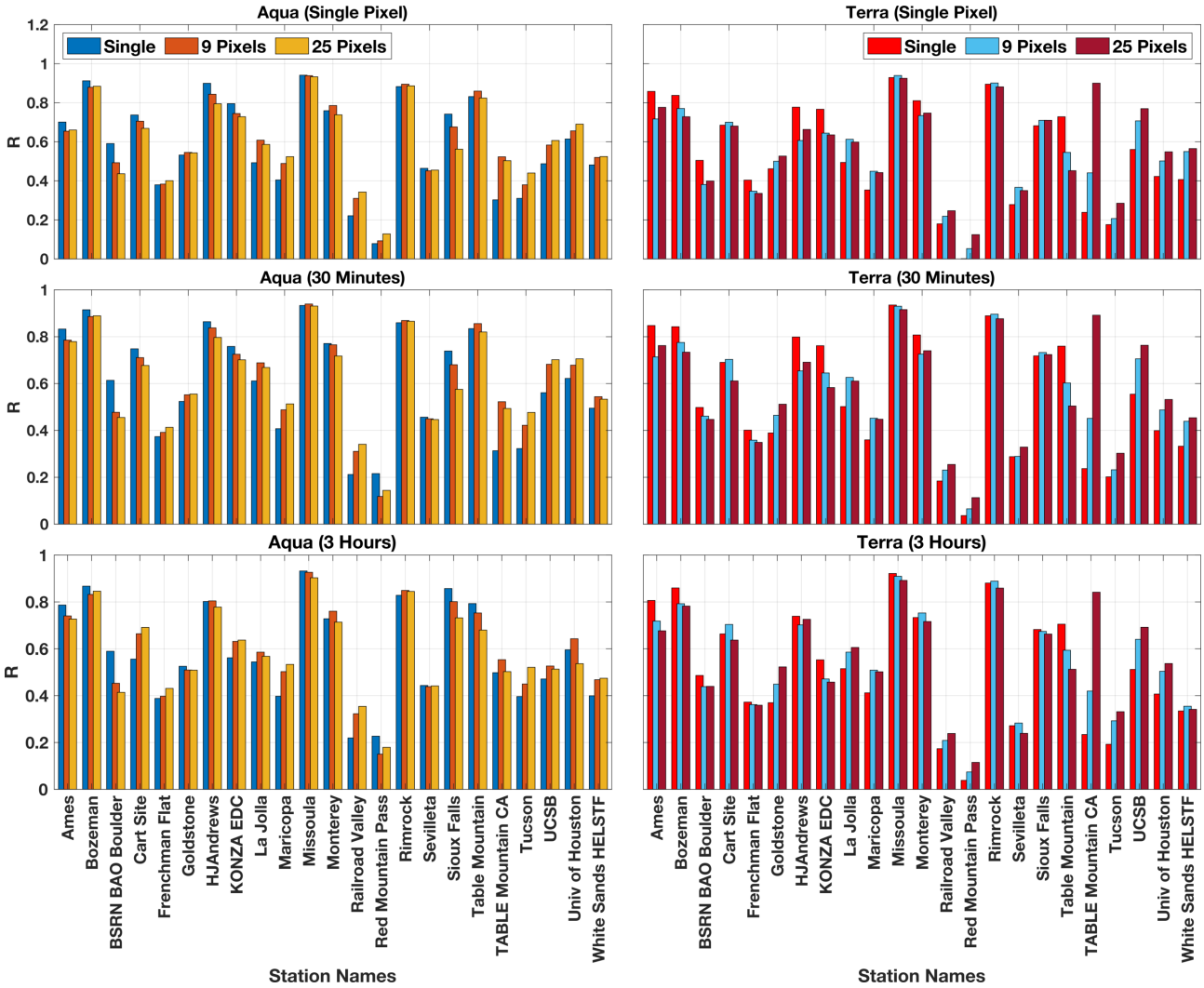


Figure 5. Pearson correlation coefficient between MODIS DB AOD (Aqua and Terra) and AERONET AOD over 23 stations at different combinations of temporal and spatial averaging domains. The actual of AODs are available in the data at that https://doi.org/10.17632/9v6pwjzxg6.1 (accessed on 11 June 2021).

During the aforementioned series of temporal changes, the number of samples also changed significantly (Table A1). The number of samples increased with an increase in temporal scales. However, the rate of change was different from site to site. The rate of change from the nearest single pixel to ±15 min ranges from 4% to 11.4% (only the White Sands HELSTF site showed a change of 115%) and from ±15 to ±90 min ranges from 9.3% to 34%. In the scenario from the nearest single pixel to ±15 min, the lowest

and highest percentage of changes happened at Goldstone station and Frenchman station, respectively. Increasing from ±15 to ±90 min, the lowest and highest percentage of change in the number of samples was shown at Railroad Valley station and White Sands HELSTF, respectively. These changes could be partly contributed by the difference in the availability of AERONET AOD records at different temporal averaging domains. The change in the number of samples either weakened or strengthened the correlation between the variables. It is worth noting that the gaps in AOD measurements between the AERONET sites might impact the correlation spectrum. Consequently, it is difficult to conclude how the rate of change in the number of matched samples influenced the relationship, as it may depend on the geographical location, aerosol type, meteorology, etc. In addition, the increase in the temporal scale caused the disappearance of the only non-significant correlation (Table A1).

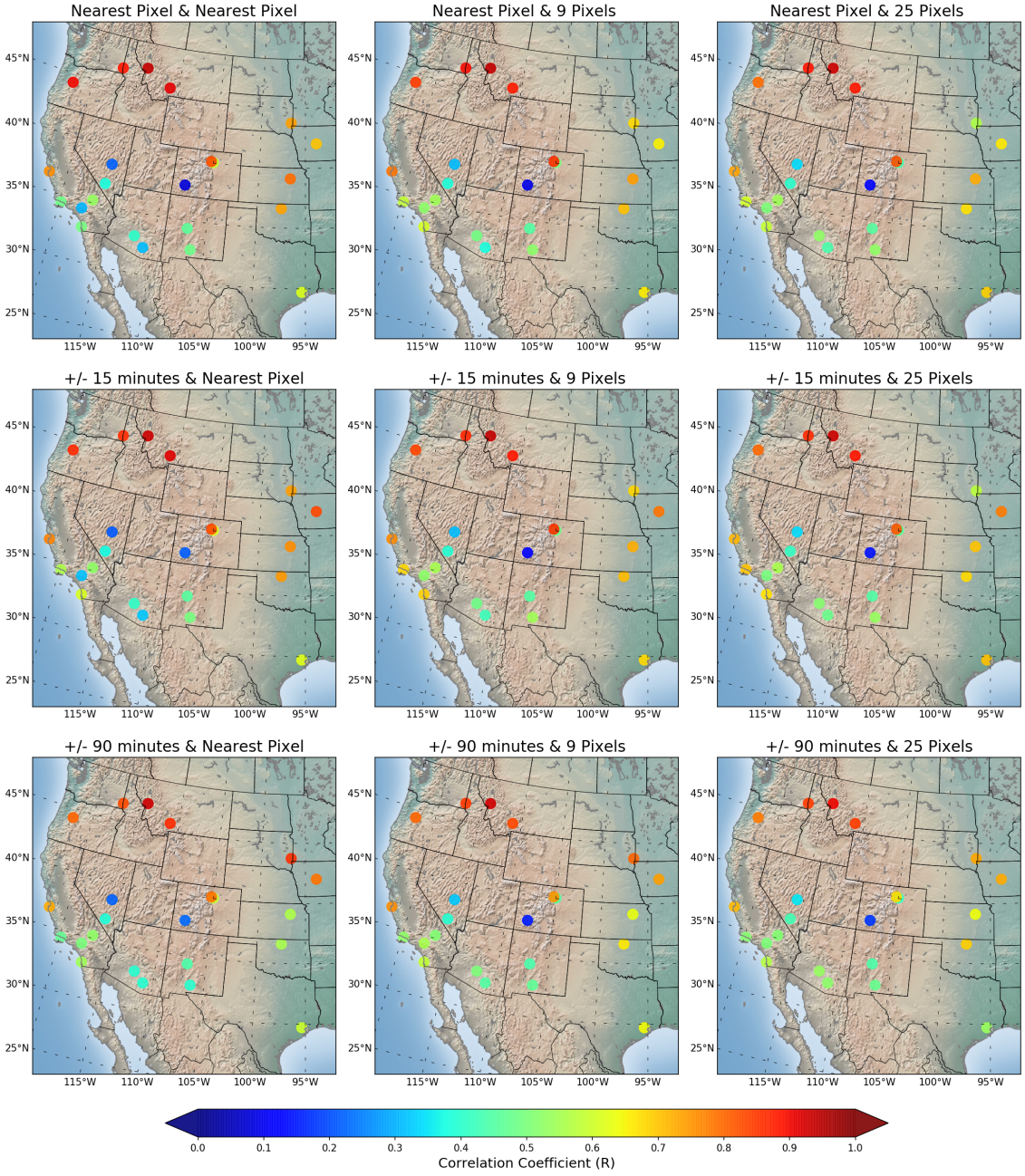


Figure 6. Pearson correlation coefficient between spatially aggregated at nearest pixel, 30 km × 30 km box and 50 km × 50 km box Aqua MODIS DB AOD and temporally aggregated at nearest, ±15 min and ±90 min AERONET AOD at 23 AERONET sites across the western United States.

Perhaps due to the difference in satellite overpass time and associated differences in the matched number of samples with AERONET AOD measurements, Terra DB AOD from the nearest single pixel (spatially) showed a significant difference with Aqua DB AOD when the temporal domain increased from the nearest single pixel to ±15 min and then to ±90 min. Twelve stations (a different set of stations as compared to Aqua) experienced an increase in the Pearson correlation coefficient when the temporal distance increased from the nearest single pixel to the ±15 min averaging extent. In eight of these stations, the correlation further increased as the temporal averaging domain increased from ±15 to ±90 min, while the remaining four stations showed a decrease in correlation. On the other hand, 11 of the stations exhibited a decreasing correlation when the temporal aggregating domain increased from the nearest single pixel to ±15 min. Extending the temporal averaging domain from ±15 to ±90 min led to nine out of the eleven stations to show further decreases in correlation, while only two stations bounced back to an increase in correlation.

Similar to the Aqua DB AOD–AERONET coupling, Terra DB AOD–AERONET coupling revealed an increase in the number of matched samples and change in the significance of correlation with an increase in temporal resolution. The percentage change of the number of samples extends from 3.6% to 12.9% and 7.4% to 31.7% when the temporal domain increases from the nearest single pixel to ±15 min and from ±15 min to ±90 min, respectively. From the nearest single pixel to ±15 min, the lowest and highest percentage of change was observed at Goldstone station and Frenchman station, respectively, stations representing the Mojave Desert ecoregion. The dynamics of these changes could have emerged from the impact of the bright desert surface on the MODIS AOD retrieval. Changing from the ±15 to ±90 min domain, the lowest and highest percentage of change occurred at Red Mountain Pass station and Rimrock station, respectively.

From the investigation of the Pearson correlation coefficient between Aqua DB AOD aggregated using a 30 km × 30 km box and AERONET AOD, 14 stations showed an increase in correlation when the temporal extent increased from the nearest single pixel to ±15 min (Figure 5). These stations represent a wide range of ecoregions. This finding suggests that over these 14 stations a major fraction of the aerosols may have been in suspension for a long period of time or the aerosol sources were continually injecting aerosols into the atmosphere. The other nine stations showed a decreasing correlation. This decrease in correlation could be linked to the dispersion or settlement of aerosol particles from the atmosphere. Extending temporal domains from ±15 min to ±90 min resulted in a decline of correlation over 16 stations. This observation indicates that as the spatiotemporal averaging domains for AERONET AOD increase, the relationship between both variables starts to diminish. When the time interval increased from the nearest single pixel to ±15 min, the lowest and highest percentage change of the number of samples were observed at the Bozeman station with 4.6% and the Frenchman Flat station with 12.1%, respectively. As the temporal aggregation is associated with the AERONET AOD data, this spectrum in the rate of change could be linked to the availability of data before and after the satellite overpass time. Increasing the temporal extent from ±15 min to ±90 min, the number of samples quadrupled compromising the strength of correlation coefficients. The lowest and highest correlation was observed at the Goldstone station with 14.5% and the Rimrock station with 46.5%, respectively (Table A1).

Terra MODIS DB AOD aggregated using a 30 km × 30 km box showed an increase in correlation at 14 stations when compared with AERONET AOD when the temporal extent increased from the nearest single pixel to ±15 min. The remaining nine stations experienced a decrease in correlation. With an increase in the temporal averaging range from ±15 to ±90 min, 13 stations exhibited a decrease in correlation, while the rest of the stations showed an increase in correlation. From the nearest single pixel to ±15 min, the lowest and highest percentage of change occurred for the number of samples at the Goldstone station with 4.8% and at the Frenchman Flat station with 13.6%, respectively. Changing from ±15 min to ±90 min, the lowest and highest percentage of change observed

in the number of samples at the Goldstone station with 15.9% and at the Ames station with 42.4%, respectively.

Aqua MODIS DB AOD averaged using a 50 km × 50 km box (corresponding to 5 pixels × 5 pixels) was also compared with AERONET AOD processed at the nearest single pixel, ±15 min and ±90 min to the Aqua MODIS overpass time. As in the previous scenarios, the ±15 min for aggregating AERONET AOD showed a better performance in improving the correlation coefficient. Fourteen stations displayed an increase in correlation when the aggregation of AERONET AOD increased from the nearest single pixel to ±15 min. A further increase to ±90 min led to a decrease in correlation in 13 stations and an increase in 15 stations. This finding indicated that with coarser spatiotemporal domains (50 km × 50 km box and ±90 min) the correlation strength was diminished by the AOD values acquired from distant pixels in time and space. In other words, with a further increase in the spatiotemporal scale the pixels start to decrease their representation with the center of the box. The Bozeman station (4.9%) showed the lowest percentage of change in the number of samples and the University of Houston station (13.6%) the highest when increased from the nearest single pixel to ±15 min. The heterogeneity of geographical location, land cover/land use setting, and sources of aerosols in both these stations could be attributed to the variability. However, when the temporal domain increased from ±15 min to ±90 min, the Goldstone station saw the lowest (16.8%) and the Rimrock station the highest (52%).

Furthermore, the correlation coefficient between Aqua DB AOD and AERONET AOD exhibited large regional variability across the western United States. In particular, the correlation coefficient values in the stations from the southwestern United States were relatively lower than those in other regions of the study area across all spatiotemporal scenarios, with the exception of the Red Mountain Pass station (Figure 6). The stations in the northern part of the study area displayed the strongest correlation. The correlation between Terra DB AOD and AERONET AOD showed the same distribution pattern of correlation as the Aqua MODIS DB AOD–AERONET AOD coupling, however, slightly lower in strength. The Railroad Valley and Red Mountain stations showed the lowest correlation at all temporal and spatial domains.

The latitudinal differences in the correlation between MODIS and AERONET AOD in the western United States may be primarily a manifestation of uncertainty in the satellite-retrieved AOD from MODIS. Given its areas of bright surface reflectance where it is difficult for the satellite to separate the surface from the atmospheric signal, the desert regions of southwest North America provide challenges for accurate satellite retrievals. This would result in reduced correlations in the southwestern regions of the United States (Thomas F. Eck, personal communication, 2021). Additionally, the prevalence of large forest fires in the northwestern United States result in high AOD values, and the correlation often improves when the AOD data range is larger. This factor likely increases the correlation in the northern latitudes (Thomas F. Eck, personal communication, 2021). Furthermore, the accuracy of the AERONET-measured AOD is very high at around 0.01 (around 0.02 in ultraviolet) for the overhead sun [59,60]. This accuracy is even better at larger zenith angles, therefore there is some improvement in the accuracy of AERONET-measured AOD at higher latitudes.

The AOD measurement at 550 nm from the MODIS DT aboard Aqua and Terra satellites was evaluated against AERONET AOD. The results from this comparison were also compared with the correlation coefficient from the MODIS DB AOD–AERONET AOD coupling, with the objective to identify the product that better characterizes the atmospheric aerosol loading across the western United States. We used the AOD at 550 nm retrieved from land and ocean through the DT algorithm with the scientific data name of "Optical_Depth_Land_And_Ocean". The results for the evaluation of the MODIS DT AOD are presented in Figure 7–9 and Table A2.

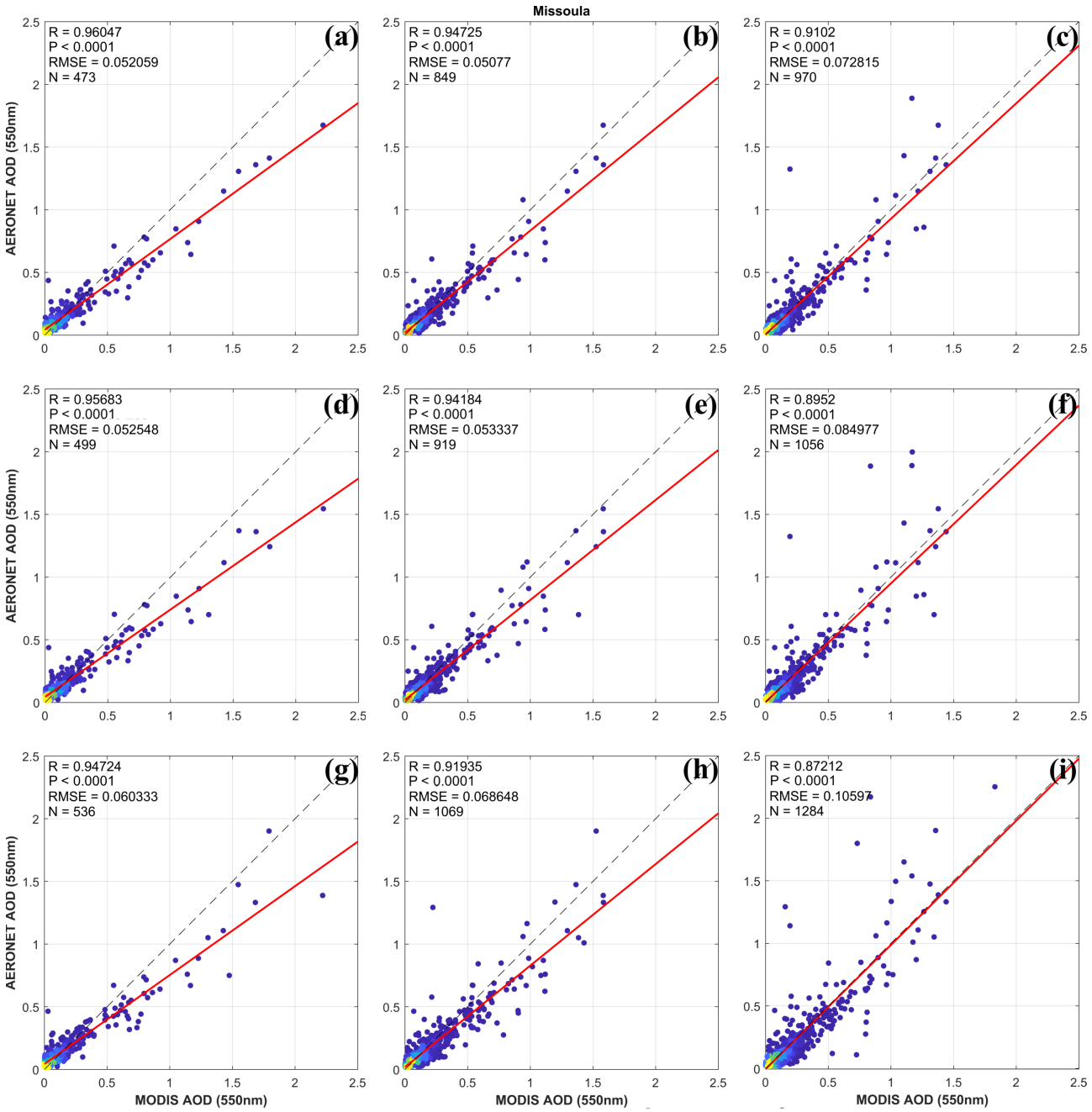


Figure 7. Scatter plots representing the validation of Aqua MODIS DT (land and ocean) AOD against AERONET AOD processed at 550 nm of the representative Missoula station: Nearest single pixel in time (**a**) nearest single pixel in space, averaged from nearest (**b**) 9 pixels, and (**c**) 25 pixels; 30 min averaging domain (**d**) nearest single pixel in time, averaged from nearest (**e**) 9 pixels, and (**f**) 25 pixels; and 3-h averaging domain (**g**) nearest single pixel in time, averaged from nearest (**h**) 9 pixels, and (**i**) 25 pixels. The red line is a regression line. Where R—Pearson correlation coefficient, P—*p* value, RMSE—root mean square error at 5% significance level, and N—number of matched AOD points.

Generally, the MODIS DT AOD showed better correlation with AERONET AOD across all spatiotemporal domains and all ecoregions as compared with the MODIS DB AOD. For example, Missoula station scored a correlation coefficient of 0.960 in the Aqua DT AOD–AERONET AOD comparison acquired from the nearest pixel in space and time (Figure 7). However, in the case of Aqua DB AOD and AERONET AOD comparisons it recorded a correlation coefficient of 0.941 (Figure 4). Similar patterns of correlation differences were observed across all the remaining spatiotemporal settings. The University of Houston station, in a coastal and urban environment showed a percentage change

increase of 55% going from Aqua DB AOD (0.612) to Aqua DT AOD (0.952) from the nearest single pixel in space and time. The inclusion of land and ocean pixels in the DT algorithm could have partly influenced the strength of the correlation. In addition, an increase in correlation from DB to DT in the coastal stations of Monterey and UCSB to those from central California may be partly contributed by the presence of more vegetated surface and sea salt aerosol presence that was commensurate with the merits of the DT algorithm [61]. The Maricopa site showed the lowest correlation between Aqua DT AOD acquired from the nearest pixel in space and AERONET AOD aggregated from the nearest pixel, ±15 min, and ±90 min (Figure 9). This is due to an insufficient number of matched data points (Table A2). Sayer et al. [50] suggested that the difference in correlation between DB AOD–AERONET AOD and DT AOD–AERONET AOD couplings was linked to the persistently low AOD measurements, tricky surface conditions, and algorithmic assumptions. According to their global-scale study, southwest North America was one of the few regions that showed the largest differences in seasonal mean AOD between DB AOD and DT AOD.

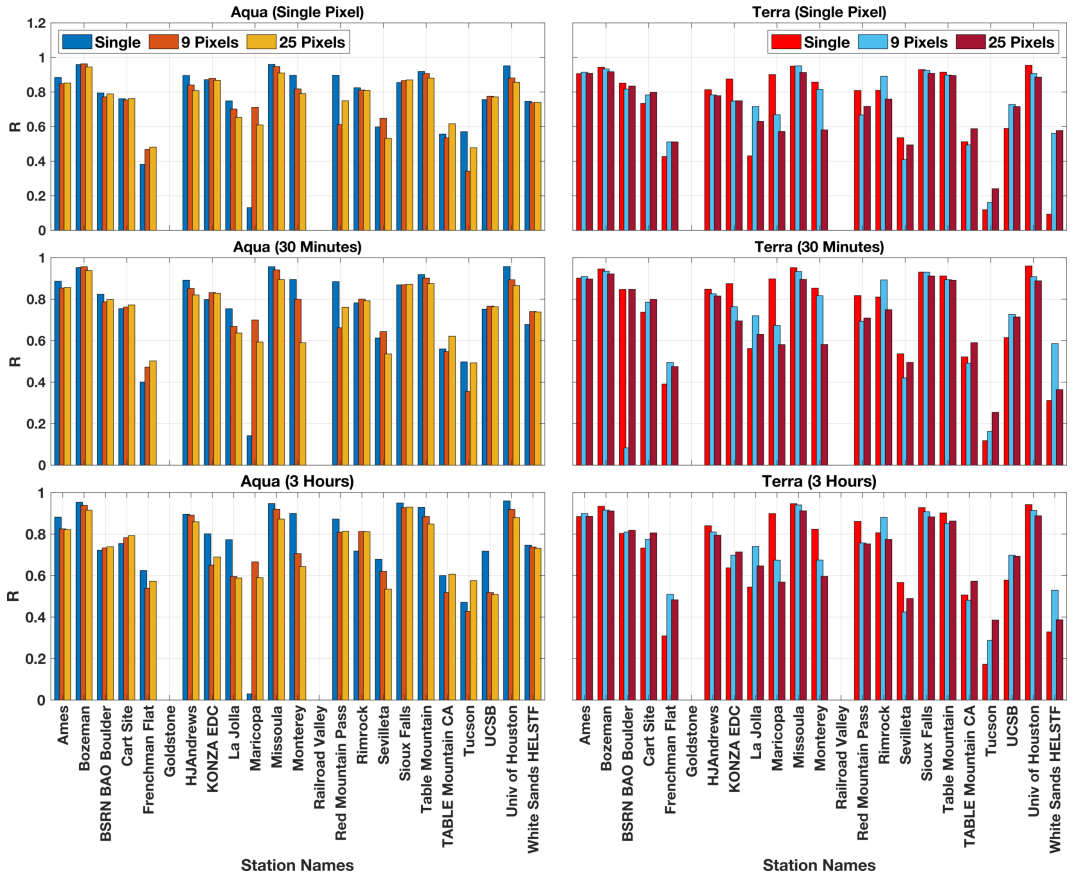


Figure 8. Pearson correlation coefficient between MODIS (Aqua and Terra) DT AOD (land and ocean) and AERONET AOD over 23 stations at different combinations of temporal and spatial averaging domains.

MODIS DT AOD exhibited a significant percentage decrease on the matched number of samples with AERONET AOD as compared with MODIS DB AOD. This change occurred at all stations and across all temporal and spatial scenarios. More specifically, the stations from the southwest United States (Frenchman Flat, Maricopa, Sevilleta, Tucson, and White Sands HELSTF), coastal regions (La Jolla, UCSB, and University of Houston), and Colorado Rocky Mountains (Red Mountain Pass) showed a decrease greater than 89% (Table A1 and A2). This pattern supports the strength of the DB algorithm in retrieving aerosol parameters in arid and semi-arid regions and alpine environments. However, despite lower numbers of matched samples, MODIS DT AOD showed a higher correlation

with AERONET AOD in a majority of the stations. The Goldstone and Railroad Valley stations from the southwest never showed matched samples for the DT product.

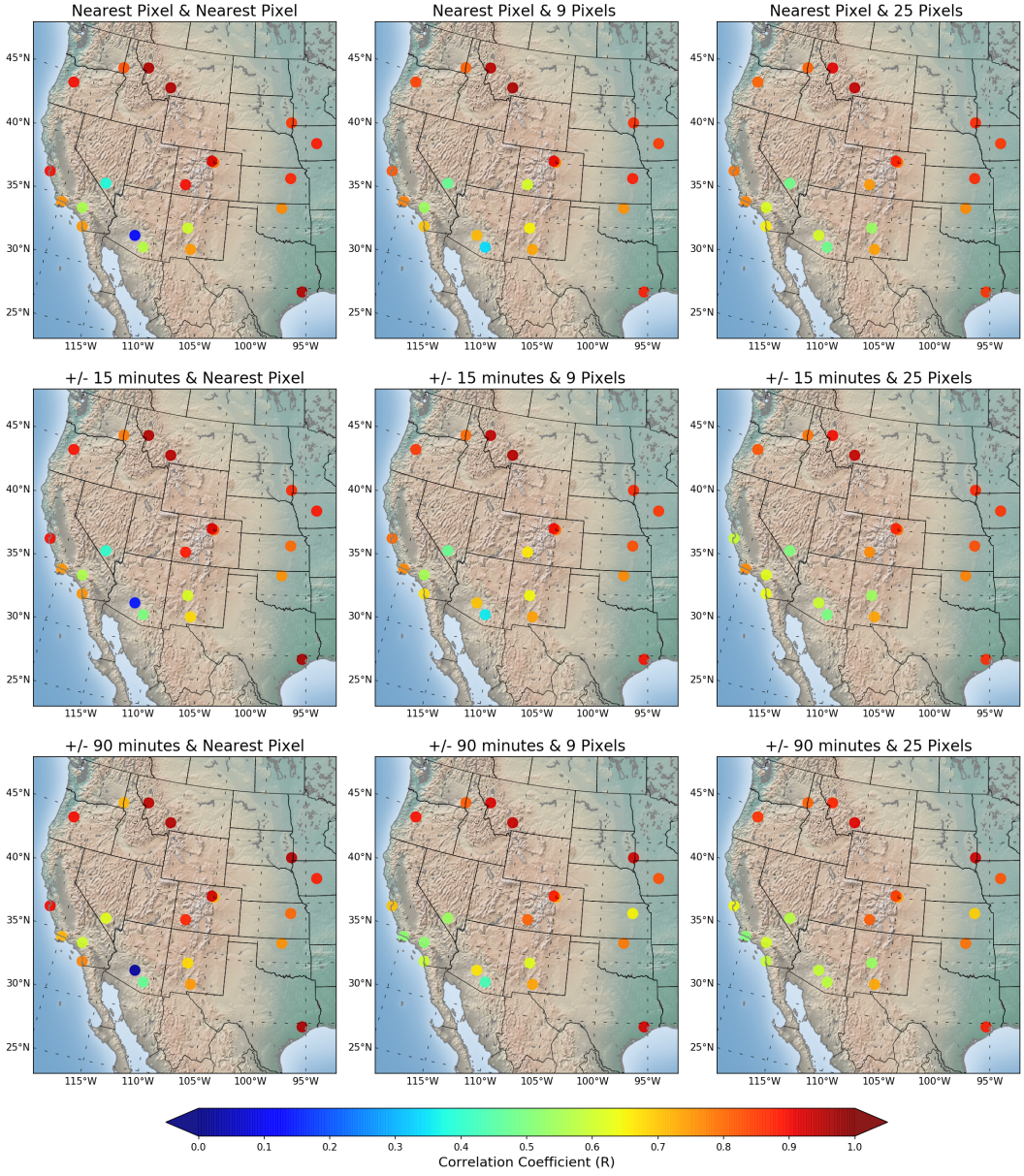


Figure 9. Pearson correlation coefficients between spatially aggregated at the nearest pixel, 30 km × 30 km box, and 50 km × 50 km box Aqua MODIS DT (Land and Ocean) AOD and temporally aggregated at the nearest ±15 min and ±90 min AERONET AOD at 23 AERONET sites across the western United States.

6. Discussion

In summary, this study demonstrated that the augmentation of aerosol optical depth data products from satellite remote sensing and ground-based platforms can improve the characterization of aerosol loading in space and time across the western United States. Monthly and seasonal maps exhibited a wide range of MODIS aerosol optical parameter retrievals and identified the time periods impacted by the data gaps. These maps can be used as a reference for spotting the temporal and spatial spaces during the process of location selection for the deployment of ground-based instruments to augment satellite remote sensing measurements. We evaluated the MODIS Level 2 AOD from DB and DT retrieval algorithms using a ground-based remote sensing product of AOD from AERONET

by utilizing different spatiotemporal aggregation domains using the coordinate information of the 23 AERONET sites as a centroid for aggregation. The findings from this analysis can help in the calibration of MODIS aerosol retrieval algorithms in the locations where their correlation with AERONET AOD were very low, such as the southwestern United States. In addition, it can provide information about the performance of AERONET sites.

Although MODIS Level 2 (10 km × 10 km) aerosol products are available at a better spatial resolution than Level MODIS Level 3 (1° × 1°) almost all the studies similar to the current study focusing in the United States utilized used MODIS Level 3 gridded aerosol data. This is because the quantitative use of Level 2 aerosol data requires a significant level of expertise in aerosol remote sensing, computer programming, and computing resources [62]. However, the current study is the first of its kind to utilize MODIS Level 2 aerosol data products at finer and multiple spatiotemporal aggregating domains involving 23 ground stations distributed at different topographic and climatic conditions of the western United States. In addition, no single study has been conducted to compare MODIS and AERONET aerosol products that are apparently focusing over the sub-continental western United States. In the previous studies, the western United States has been considered under coarser scales, either a continental [63] or global scale [62,64]. A continental study by Drury et al. [63] reported a correlation coefficient of 0.32 (R = 0.32) between MODIS and AERONET AOD in the western and central United States using a daily data for the period of 1 July–15 August 2004; although their correlation increased to 0.64 with a weekly averaging domain. Our study utilized the available resource of a finer temporal resolution of both data products in order to capture the dynamic nature of aerosol loading influenced by topographic and climatic conditions. On a regional scale, Loria-Salazar et al. [61] evaluated the MODIS Collection 6.0 aerosol product using an AERONET product in semi-arid Nevada and California, United States, during the summer of 2012. Similar to our results, their study found a weak correlation between both data products, a correlation coefficient of 0.316–0.447 during non-fire periods, and 0–0.557 during fire periods. However, our study covers 17 years of aerosol data records.

7. Conclusions

The current study contributes a comprehensive approach to the evaluation of remotely sensed satellite aerosol products using ground-based aerosol products by utilizing different aggregating domains covering a very large study area, different land cover/land use settings, and geographical locations. Overall, this study demonstrated that the augmentation of aerosol data products from satellite remote sensing and ground-based platforms can improve the characterization of aerosol loading in space and time across the western United States. It explored deeper into the finer temporal and spatial scenarios than previous studies by optimizing the aggregating approaches performing the long-term inventory of the aerosol data records from both the satellite and ground-based platforms. In order to assess the variability of aerosol concentrations in space and time from the AERONET sites, the study integrated high aggregating domains. Based on these in-depth approaches, this study identified stations and regions with a strong potential for evaluating and calibrating satellite products, and spotted stations and regions that showed avery low correlation with the satellite observation and stations with many data gaps and few data records.

In general, the majority of the stations revealed a significant correlation between MODIS and AERONET AOD at all spatiotemporal aggregating domains. Specifically, the stations from the higher latitude sites showed a stronger correlation, making the sites suitable for evaluating satellite retrievals. However, the stations from the southwestern United States desert showed the lowest correlation coefficients. In view of this region being a dominant source of mineral dust, these findings suggest that the MODIS AOD should be further improved and locally calibrated. Aerosol sources, such as windblown dust and anthropogenic fugitive dust (e.g., road dust from unpaved road), are short-lived and heterogeneous over space and time. Such source characteristics, along with bright, reflective desert surface, make it particularly challenging for satellite retrievals in this region. We

recommend the application of medium spatiotemporal collocating resolutions (temporally ±15 min and spatially 30 km × 30 km) for the estimation of ground-based air quality parameters. Incorporating aerosol products from geostationary satellites like NASA's Geostationary Operational Environmental-16 (GOES-16) Advanced Baseline Imager (ABI) into the dataset used in this study can significantly improve the characterization of the aerosol loading and air quality assessment rather than using MODIS- and AERONET-derived AOD only. Aerosol products from GOES-16 ABI possess a higher temporal resolution than MODIS and they can mitigate the sparseness of aerosol observations from MODIS-AERONET couplings. More investigations are needed to understand the aerosol impacts of long-term land cover and land use changes around AERONET sites as these surface types are very sensitive to climate change and variability, and this parameter in turn is crucial in determining the response of the land-surface-to-satellite signals.

Author Contributions: Conceptualization, I.G.E. and T.E.G.; Methodology, I.G.E. and T.E.G.; Software, I.G.E.; Validation, I.G.E., T.E.G., R.S.V.P., and D.Q.T.; Formal analysis, I.G.E. and T.E.G.; Investigation, I.G.E. and T.E.G.; Resources, I.G.E., T.E.G., D.Q.T., and R.S.V.P.; Data curation, I.G.E.; Writing—original draft preparation, I.G.E., T.E.G., R.S.V.P., and D.Q.T.; Writing—review and editing, I.G.E., T.E.G., R.S.V.P., and D.Q.T.; Visualization, I.G.E.; Supervision, T.E.G., R.S.V.P., and D.Q.T.; Project administration, T.E.G.; Funding acquisition, T.E.G. and D.Q.T. All authors have read and agreed to the published version of the manuscript.

Funding: This research was funded by NASA, grant numbers NNX16AH13G and 80NSSC19K0195.

Institutional Review Board Statement: Not applicable.

Informed Consent Statement: Not applicable.

Data Availability Statement: Refer to doi: https://doi.org/10.17632/9v6pwjzxg6.1 (accessed on 11 June 2021).

Acknowledgments: The authors would like to thank the National Aeronautics and Space Administration (NASA) for providing MODIS Level 2 Aerosol Products Collection 6.1 from Terra and Aqua satellites, the Aerosol Robotic Network (AERONET), and the principal investigators of the 23 AERONET sites for allowing us to use ground-based Level 2 aerosol data products, the United States Environmental Protection Agency (EPA) for the ecological classification map of the United States, and the United States Geological Survey (USGS) for the digital elevation model (DEM). The authors acknowledge Carlos Montana of the Department of Earth, Environmental, and Resource Sciences from the University of Texas at El Paso. We also acknowledge Thomas F. Eck, Santiago Gasso, and Robert Levy for their helpful comments.

Conflicts of Interest: The authors declare no conflict of interest. USDA is an equal opportunity employer and provider. Mention of trade names is for information purposes only and does not infer endorsement by or exclusion of equivalent products by USDA.

Abbreviations

The following abbreviations are used in this manuscript:

AOD	Aerosol Optical Depth
AERONET	Aerosol Robotic Network
MODIS	Moderate Resolution Imaging SpectroRadiometer
DB	Deep Blue
DT	Dark Target
GOCI	Geostationary Ocean Color Imager
MISR	Multi-angle Imaging SpectroRadiometer
SeaWiFS	Sea-viewing Wide Field-of-view Sensor
OMI	Ozone Monitoring Instrument
USGS	United States Geological Survey
NASA	National Aeronautics and Space Administration
USDA	United States Department of Agriculture
GOES	Geostationary Operational Environmental
ABI	Advanced Baseline Imager

Appendix A

Table A1. *p*-value and number of matched samples between MODIS DB AOD (Aqua and Terra) and AERONET AOD of 23 sites across western United States at different combinations of temporal and spatial averaging domains. The yellow shaded cells represent a not significant correlation.

Site ID	Nearest in Time						30 Minutes Averaging Domain						3 Hours Averaging Domain					
	Single		9 Pixels		25 Pixels		Single		9 Pixels		25 Pixels		Single		9 Pixels		25 Pixels	
	Aqua	Terra	Aqua	Terra	Aqua	Terra	Aqua	Terra	Aqua	Terra	Aqua	Terra	Aqua	Terra	Aqua	Terra	Aqua	Terra
St. 1	<0.05	<0.05	<0.05	<0.05	<0.05	<0.05	<0.05	<0.05	<0.05	<0.05	<0.05	<0.05	<0.05	<0.05	<0.05	<0.05	<0.05	<0.05
	488	473	594	608	644	642	540	521	672	668	729	713	709	681	953	951	1083	1055
St. 2	<0.05	<0.05	<0.05	<0.05	<0.05	<0.05	<0.05	<0.05	<0.05	<0.05	<0.05	<0.05	<0.05	<0.05	<0.05	<0.05	<0.05	<0.05
	749	769	1027	1038	1092	1116	780	798	1074	1091	1146	1182	873	874	1303	1302	1461	1465
St. 3	<0.05	<0.05	<0.05	<0.05	<0.05	<0.05	<0.05	<0.05	<0.05	<0.05	<0.05	<0.05	<0.05	<0.05	<0.05	<0.05	<0.05	<0.05
	1113	1233	1465	1682	1584	1734	1184	1305	1600	1804	1740	1865	1420	1531	2116	2316	2409	2473
St. 4	<0.05	<0.05	<0.05	<0.05	<0.05	<0.05	<0.05	<0.05	<0.05	<0.05	<0.05	<0.05	<0.05	<0.05	<0.05	<0.05	<0.05	<0.05
	1281	1301	1685	1661	1836	1817	1369	1387	1820	1788	1989	1959	1612	1617	2283	2204	2568	2492
St. 5	<0.05	<0.05	<0.05	<0.05	<0.05	<0.05	<0.05	<0.05	<0.05	<0.05	<0.05	<0.05	<0.05	<0.05	<0.05	<0.05	<0.05	<0.05
	736	734	907	884	930	904	820	829	1017	1004	1044	1025	1055	1038	1370	1330	1431	1372
St. 6	<0.05	<0.05	<0.05	<0.05	<0.05	<0.05	<0.05	<0.05	<0.05	<0.05	<0.05	<0.05	<0.05	<0.05	<0.05	<0.05	<0.05	<0.05
	985	924	1172	1134	1215	1155	1024	957	1229	1188	1276	1212	1127	1071	1407	1377	1490	1430
St. 7	<0.05	<0.05	<0.05	<0.05	<0.05	<0.05	<0.05	<0.05	<0.05	<0.05	<0.05	<0.05	<0.05	<0.05	<0.05	<0.05	<0.05	<0.05
	724	670	843	833	857	853	773	719	910	898	927	922	904	831	1115	1063	1158	1112
St. 8	<0.05	<0.05	<0.05	<0.05	<0.05	<0.05	<0.05	<0.05	<0.05	<0.05	<0.05	<0.05	<0.05	<0.05	<0.05	<0.05	<0.05	<0.05
	806	818	1037	1072	1123	1106	870	880	1125	1158	1232	1197	1063	1051	1471	1490	1645	1583
St. 9	<0.05	<0.05	<0.05	<0.05	<0.05	<0.05	<0.05	<0.05	<0.05	<0.05	<0.05	<0.05	<0.05	<0.05	<0.05	<0.05	<0.05	<0.05
	679	635	891	808	916	825	734	681	967	876	995	896	930	848	1277	1154	1342	1202
St. 10	<0.05	<0.05	<0.05	<0.05	<0.05	<0.05	<0.05	<0.05	<0.05	<0.05	<0.05	<0.05	<0.05	<0.05	<0.05	<0.05	<0.05	<0.05
	775	651	954	822	982	841	813	685	1009	865	1044	886	997	841	1261	1104	1322	1140
St. 11	<0.05	<0.05	<0.05	<0.05	<0.05	<0.05	<0.05	<0.05	<0.05	<0.05	<0.05	<0.05	<0.05	<0.05	<0.05	<0.05	<0.05	<0.05
	909	1191	1223	1388	1318	1484	981	1260	1352	1490	1464	1605	1167	1477	1801	1901	2030	2116
St. 12	<0.05	<0.05	<0.05	<0.05	<0.05	<0.05	<0.05	<0.05	<0.05	<0.05	<0.05	<0.05	<0.05	<0.05	<0.05	<0.05	<0.05	<0.05
	1150	883	1384	1106	1405	1163	1211	936	1471	1172	1492	1233	1410	1134	1758	1500	1810	1609
St. 13	<0.05	<0.05	<0.05	<0.05	<0.05	<0.05	<0.05	<0.05	<0.05	<0.05	<0.05	<0.05	<0.05	<0.05	<0.05	<0.05	<0.05	<0.05
	861	1190	2003	2003	2155	2160	903	1251	2140	2121	2308	2291	987	1382	2528	2507	2799	2768
St. 14	>0.05	>0.05	<0.05	>0.05	<0.05	<0.05	<0.05	>0.05	<0.05	>0.05	<0.05	<0.05	<0.05	>0.05	<0.05	<0.05	<0.05	<0.05
	123	163	486	529	663	722	131	176	535	591	742	828	153	189	680	742	1033	1126
St. 15	<0.05	<0.05	<0.05	<0.05	<0.05	<0.05	<0.05	<0.05	<0.05	<0.05	<0.05	<0.05	<0.05	<0.05	<0.05	<0.05	<0.05	<0.05
	1000	976	1237	1227	1272	1338	1095	1086	1373	1372	1412	1501	1469	1430	2012	1941	2147	2157
St. 16	<0.05	<0.05	<0.05	<0.05	<0.05	<0.05	<0.05	<0.05	<0.05	<0.05	<0.05	<0.05	<0.05	<0.05	<0.05	<0.05	<0.05	<0.05
	1232	1390	1545	1744	1644	1842	1305	1471	1664	1862	1771	1969	1526	1676	2105	2223	2312	2391
St. 17	<0.05	<0.05	<0.05	<0.05	<0.05	<0.05	<0.05	<0.05	<0.05	<0.05	<0.05	<0.05	<0.05	<0.05	<0.05	<0.05	<0.05	<0.05
	845	895	1086	1110	1144	1176	918	958	1190	1196	1259	1271	1114	1132	1557	1548	1731	1697
St. 18	<0.05	<0.05	<0.05	<0.05	<0.05	<0.05	<0.05	<0.05	<0.05	<0.05	<0.05	<0.05	<0.05	<0.05	<0.05	<0.05	<0.05	<0.05
	695	861	965	1077	999	1147	738	909	1051	1152	1098	1225	857	1020	1374	1424	1528	1583
St. 19	<0.05	<0.05	<0.05	<0.05	<0.05	<0.05	<0.05	<0.05	<0.05	<0.05	<0.05	<0.05	<0.05	<0.05	<0.05	<0.05	<0.05	<0.05
	1021	1035	1343	1353	1433	1430	1087	1094	1447	1438	1542	1523	1283	1276	1809	1756	1957	1880
St. 20	<0.05	<0.05	<0.05	<0.05	<0.05	<0.05	<0.05	<0.05	<0.05	<0.05	<0.05	<0.05	<0.05	<0.05	<0.05	<0.05	<0.05	<0.05
	512	535	647	639	665	692	538	561	692	671	714	726	624	660	828	833	882	914

Table A1. *Cont.*

Site ID	Nearest in Time						30 Minutes Averaging Domain						3 Hours Averaging Domain					
	Single		9 Pixels		25 Pixels		Single		9 Pixels		25 Pixels		Single		9 Pixels		25 Pixels	
	Aqua	Terra	Aqua	Terra	Aqua	Terra	Aqua	Terra	Aqua	Terra	Aqua	Terra	Aqua	Terra	Aqua	Terra	Aqua	Terra
St. 21	<0.05	<0.05	<0.05	<0.05	<0.05	<0.05	<0.05	<0.05	<0.05	<0.05	<0.05	<0.05	<0.05	<0.05	<0.05	<0.05	<0.05	<0.05
	956	833	1365	1246	1421	1273	1018	885	1454	1321	1513	1357	1225	1046	1834	1664	1926	1736
St. 22	<0.05	<0.05	<0.05	<0.05	<0.05	<0.05	<0.05	<0.05	<0.05	<0.05	<0.05	<0.05	<0.05	<0.05	<0.05	<0.05	<0.05	<0.05
	491	440	664	660	778	728	530	476	744	731	884	811	592	547	947	930	1195	1089
St. 23	<0.05	<0.05	<0.05	<0.05	<0.05	<0.05	<0.05	<0.05	<0.05	<0.05	<0.05	<0.05	<0.05	<0.05	<0.05	<0.05	<0.05	<0.05
	644	1379	1531	1717	1579	1759	1387	1450	1655	1822	1714	1872	1691	1701	2113	2232	2239	2338

Table A2. *p*-value and number of matched samples between MODIS DT (land and ocean) AOD and AERONET AOD of 23 sites across western United States at different combinations of temporal and spatial averaging domains. The yellow shaded cells represent not significant correlation and green shaded cells represent no data.

Site ID	Nearest in Time						30 Minutes Averaging Domain						3 Hours Averaging Domain					
	Single		9 Pixels		25 Pixels		Single		9 Pixels		25 Pixels		Single		9 Pixels		25 Pixels	
	Aqua	Terra	Aqua	Terra	Aqua	Terra	Aqua	Terra	Aqua	Terra	Aqua	Terra	Aqua	Terra	Aqua	Terra	Aqua	Terra
St. 1	<0.05	<0.05	<0.05	<0.05	<0.05	<0.05	<0.05	<0.05	<0.05	<0.05	<0.05	<0.05	<0.05	<0.05	<0.05	<0.05	<0.05	<0.05
	265	305	383	449	437	494	286	330	429	490	495	542	331	398	542	631	655	740
St. 2	<0.05	<0.05	<0.05	<0.05	<0.05	<0.05	<0.05	<0.05	<0.05	<0.05	<0.05	<0.05	<0.05	<0.05	<0.05	<0.05	<0.05	<0.05
	558	623	783	858	841	931	566	633	807	891	873	975	588	659	881	958	1006	1087
St. 3	<0.05	<0.05	<0.05	<0.05	<0.05	<0.05	<0.05	<0.05	<0.05	<0.05	<0.05	<0.05	<0.05	<0.05	<0.05	<0.05	<0.05	<0.05
	486	650	962	1268	1109	1391	511	682	1018	1352	1184	1484	571	741	1193	1547	1464	1773
St. 4	<0.05	<0.05	<0.05	<0.05	<0.05	<0.05	<0.05	<0.05	<0.05	<0.05	<0.05	<0.05	<0.05	<0.05	<0.05	<0.05	<0.05	<0.05
	792	912	1309	1445	1480	1624	832	959	1405	1537	1598	1735	905	1030	1619	1775	1936	2078
St. 5	>0.05	<0.05	<0.05	<0.05	<0.05	<0.05	>0.05	>0.05	<0.05	<0.05	<0.05	<0.05	<0.05	>0.05	<0.05	<0.05	<0.05	<0.05
	18	23	115	137	248	276	19	25	122	148	263	310	21	30	149	186	339	378
St. 6	n/a	n/a	n/a	n/a	n/a	n/a	n/a	n/a	n/a	n/a	n/a	n/a	n/a	n/a	n/a	n/a	n/a	n/a
	n/a	n/a	n/a	n/a	n/a	n/a	n/a	n/a	n/a	n/a	n/a	n/a	n/a	n/a	n/a	n/a	n/a	n/a
St. 7	<0.05	<0.05	<0.05	<0.05	<0.05	<0.05	<0.05	<0.05	<0.05	<0.05	<0.05	<0.05	<0.05	<0.05	<0.05	<0.05	<0.05	<0.05
	580	516	728	686	756	722	604	553	773	735	805	775	650	596	866	816	930	870
St. 8	<0.05	<0.05	<0.05	<0.05	<0.05	<0.05	<0.05	<0.05	<0.05	<0.05	<0.05	<0.05	<0.05	<0.05	<0.05	<0.05	<0.05	<0.05
	608	668	846	942	937	996	636	699	907	1005	1015	1072	690	758	1064	1174	1241	1309
St. 9	<0.05	>0.05	<0.05	<0.05	<0.05	<0.05	<0.05	<0.05	<0.05	<0.05	<0.05	<0.05	<0.05	<0.05	<0.05	<0.05	<0.05	<0.05
	10	17	532	562	841	768	10	18	573	599	909	834	11	21	726	758	1203	1109
St. 10	>0.05	>0.05	<0.05	<0.05	<0.05	<0.05	>0.05	>0.05	<0.05	<0.05	<0.05	<0.05	>0.05	<0.05	<0.05	<0.05	<0.05	<0.05
	6	4	35	25	309	318	6	4	36	25	318	333	6	5	39	27	372	390
St. 11	<0.05	<0.05	<0.05	<0.05	<0.05	<0.05	<0.05	<0.05	<0.05	<0.05	<0.05	<0.05	<0.05	<0.05	<0.05	<0.05	<0.05	<0.05
	473	706	849	1016	970	1110	499	735	919	1073	1056	1174	536	792	1069	1217	1284	1394
St. 12	<0.05	<0.05	<0.05	<0.05	<0.05	<0.05	<0.05	<0.05	<0.05	<0.05	<0.05	<0.05	<0.05	<0.05	<0.05	<0.05	<0.05	<0.05
	268	266	1135	803	1305	1092	281	276	1198	837	1381	1146	302	310	1372	1018	1633	1437
St. 13	n/a	n/a	n/a	n/a	n/a	n/a	n/a	n/a	n/a	n/a	n/a	n/a	n/a	n/a	n/a	n/a	n/a	n/a
	n/a	n/a	n/a	n/a	n/a	n/a	n/a	n/a	n/a	n/a	n/a	n/a	n/a	n/a	n/a	n/a	n/a	n/a

Table A2. *Cont.*

Site ID	Nearest in Time						30 Minutes Averaging Domain						3 Hours Averaging Domain					
	Single		9 Pixels		25 Pixels		Single		9 Pixels		25 Pixels		Single		9 Pixels		25 Pixels	
	Aqua	Terra	Aqua	Terra	Aqua	Terra	Aqua	Terra	Aqua	Terra	Aqua	Terra	Aqua	Terra	Aqua	Terra	Aqua	Terra
St. 14	<0.05	>0.05	<0.05	>0.05	<0.05	<0.05	<0.05	>0.05	<0.05	>0.05	<0.05	<0.05	<0.05	>0.05	<0.05	<0.05	<0.05	<0.05
	11	20	141	190	334	396	11	21	149	204	377	447	12	22	175	236	483	574
St. 15	<0.05	<0.05	<0.05	<0.05	<0.05	<0.05	<0.05	<0.05	<0.05	<0.05	<0.05	<0.05	<0.05	<0.05	<0.05	<0.05	<0.05	<0.05
	491	577	882	991	983	1140	533	629	965	1091	1078	1264	655	760	1256	1390	1462	1658
St. 16	<0.05	<0.05	<0.05	<0.05	<0.05	<0.05	<0.05	<0.05	<0.05	<0.05	<0.05	<0.05	<0.05	<0.05	<0.05	<0.05	<0.05	<0.05
	37	46	438	631	627	821	38	48	456	658	658	859	43	50	500	716	751	959
St. 17	<0.05	<0.05	<0.05	<0.05	<0.05	<0.05	<0.05	<0.05	<0.05	<0.05	<0.05	<0.05	<0.05	<0.05	<0.05	<0.05	<0.05	<0.05
	500	616	756	877	849	969	528	641	814	933	920	1037	594	704	966	1108	1136	1298
St. 18	<0.05	<0.05	<0.05	<0.05	<0.05	<0.05	<0.05	<0.05	<0.05	<0.05	<0.05	<0.05	<0.05	<0.05	<0.05	<0.05	<0.05	<0.05
	288	470	608	769	694	895	294	492	643	810	742	949	308	505	730	894	900	1094
St. 19	<0.05	<0.05	<0.05	<0.05	<0.05	<0.05	<0.05	<0.05	<0.05	<0.05	<0.05	<0.05	<0.05	<0.05	<0.05	<0.05	<0.05	<0.05
	455	504	994	976	1230	1218	479	530	1062	1033	1318	1288	524	584	1233	1208	1572	1518
St. 20	<0.05	>0.05	<0.05	<0.05	<0.05	<0.05	<0.05	>0.05	<0.05	<0.05	<0.05	<0.05	<0.05	>0.05	<0.05	<0.05	<0.05	<0.05
	55	70	292	363	365	455	57	73	302	376	381	474	67	86	337	446	433	568
St. 21	<0.05	<0.05	<0.05	<0.05	<0.05	<0.05	<0.05	<0.05	<0.05	<0.05	<0.05	<0.05	<0.05	<0.05	<0.05	<0.05	<0.05	<0.05
	98	47	1337	1191	1418	1274	105	53	1425	1264	1510	1355	124	67	1769	1597	1907	1733
St. 22	<0.05	<0.05	<0.05	<0.05	<0.05	<0.05	<0.05	<0.05	<0.05	<0.05	<0.05	<0.05	<0.05	<0.05	<0.05	<0.05	<0.05	<0.05
	29	29	358	359	519	517	29	29	375	382	551	554	30	31	393	406	602	614
St. 23	<0.05	>0.05	<0.05	<0.05	<0.05	<0.05	<0.05	>0.05	<0.05	<0.05	<0.05	<0.05	<0.05	>0.05	<0.05	<0.05	<0.05	<0.05
	19	27	324	503	530	789	22	28	341	528	553	837	27	33	391	596	653	963

References

1. Huang, X.; Song, Y.; Zhao, C.; Cai, X.; Zhang, H.; Zhu, T. Direct radiative effect by multicomponent aerosol over China. *J. Clim.* **2015**, *28*, 3472–3495. [CrossRef]
2. Peers, F.; Waquet, F.; Cornet, C.; Dubuisson, P.; Ducos, F.; Goloub, P.; Szczap, F.; Tanré, D.; Thieuleux, F. Absorption of aerosols above clouds from POLDER/PARASOL measurements and estimation of their direct radiative effect. *Atmos. Chem. Phys.* **2015**, *15*, 4179–4196. [CrossRef]
3. Zhang, S.; Wang, M.; Ghan, S.J.; Ding, A.; Wang, H.; Zhang, K.; Neubauer, D.; Lohmann, U.; Ferrachat, S.; Takeamura, T.; et al. On the characteristics of aerosol indirect effect based on dynamic regimes in global climate models. *Atmos. Chem. Phys.* **2016**, *16*, 2765–2783. [CrossRef]
4. Jolivet, D.; Ramon, D.; Bernard, E.; Deschamps, P.Y.; Riedi, J.; Nicolas, J.M.; Hagolle, O. Aerosol monitoring over land using MSG/SEVIRI. In Proceedings of the EUMETSAT Meteorological Satellite Conference, Darmstadt, Germany, 8–12 September 2008; pp. 8–12.
5. Li, Y.; Henze, D.K.; Jack, D.; Henderson, B.H.; Kinney, P.L. Assessing public health burden associated with exposure to ambient black carbon in the United States. *Sci. Total Environ.* **2016**, *539*, 515–525. [CrossRef]
6. Shiraiwa, M.; Ueda, K.; Pozzer, A.; Lammel, G.; Kampf, C.J.; Fushimi, A.; Enami, S.; Arangio, A.M.; Fröhlich-Nowoisky, J.; Fujitani, Y.; et al. Aerosol Health Effects from Molecular to Global Scales. *Environ. Sci. Technol.* **2017**, *51*, 13545–13567. [CrossRef] [PubMed]
7. Reisen, F.; Meyer, C.P.M.; Keywood, M.D. Impact of biomass burning sources on seasonal aerosol air quality. *Atmos. Environ.* **2013**, *67*, 437–447. [CrossRef]
8. Viana, M.; Hammingh, P.; Colette, A.; Querol, X.; Degraeuwe, B.; de Vlieger, I.; van Aardenne, J. Impact of maritime transport emissions on coastal air quality in Europe. *Atmos. Environ.* **2014**, *90*, 96–105. [CrossRef]
9. Gao, M.; Guttikunda, S.K.; Carmichael, G.R.; Wang, Y.; Liu, Z.; Stanier, C.O.; Saide, P.E.; Yu, M. Health impacts and economic losses assessment of the 2013 severe haze event in Beijing area. *Sci. Total Environ.* **2015**, *511*, 553–561. [CrossRef] [PubMed]
10. Chin, M.; Diehl, T.; Ginoux, P.; Malm, W. Intercontinental transport of pollution and dust aerosols: Implications for regional air quality. *Atmos. Chem. Phys.* **2007**, *7*, 5501–5517. [CrossRef]
11. Schlosser, J.S.; Braun, R.A.; Bradley, T.; Dadashazar, H.; MacDonald, A.B.; Aldhaif, A.A.; Aghdam, M.A.; Mardi, A.H.; Xian, P.; Sorooshian, A. Analysis of aerosol composition data for western United States wildfires between 2005 and 2015: Dust emissions, chloride depletion, and most enhanced aerosol constituents. *J. Geophys. Res. Atmos.* **2017**, *122*, 8951–8966. [CrossRef]
12. Tong, D.Q.; Wang, J.X.L.; Gill, T.E.; Lei, H.; Wang, B. Intensified dust storm activity and Valley fever infection in the southwestern United States. *Geophys. Res. Lett.* **2017**, *44*, 4304–4312. [CrossRef]
13. Brahney, J.; Ballantyne, A.P.; Sievers, C.; Neff, J.C. Increasing Ca^{2+} deposition in the western US: The role of mineral aerosols. *Aeolian Res.* **2013**, *10*, 77–87. [CrossRef]
14. Hand, J.L.; White, W.H.; Gebhart, K.A.; Hyslop, N.P.; Gill, T.E.; Schichtel, B.A. Earlier onset of the spring fine dust season in the southwestern United States. *Geophys. Res. Lett.* **2016**, *43*, 4001–4009. [CrossRef]
15. Dennison, P.E.; Brewer, S.C.; Arnold, J.D.; Moritz, M.A. Large wildfire trends in the western United States, 1984–2011. *Geophys. Res. Lett.* **2014**, *41*, 2928–2933. [CrossRef]
16. Littell, J.S.; Mckenzie, D.; Peterson, D.L.; Westerling, A.L. Climate and wildfire area burned in western U.S. ecoprovinces, 1916–2003. *Ecol. Appl.* **2009**, *19*, 1003–1021. [CrossRef]
17. Liu, J.C.; Mickley, L.J.; Sulprizio, M.P.; Dominici, F.; Yue, X.; Ebisu, K.; Anderson, G.B.; Khan, R.F.; Bravo, M.A.; Bell, M.L. Particulate air pollution from wildfires in the Western US under climate change. *Clim. Chang.* **2016**, *138*, 655–666. [CrossRef] [PubMed]
18. McClure, C.D.; Jaffe, D.A. US particulate matter air quality improves except in wildfire-prone areas. *Proc. Natl. Acad. Sci. USA* **2018**, *115*, 7901–7906. [CrossRef] [PubMed]
19. Harvey, B.J. Human-caused climate change is now a key driver of forest fire activity in the western United States. *Proc. Natl. Acad. Sci. USA* **2016**, *113*, 11649–11650. [CrossRef] [PubMed]
20. Chung, C.E.; Ramanathan, V.; Kim, D.; Podgorny, I.A. Global anthropogenic aerosol direct forcing derived from satellite and ground-based observations. *J. Geophys. Res. Atmos.* **2005**, *110*, 1–17. [CrossRef]
21. Van Donkelaar, A.; Martin, R.V.; Pasch, A.N.; Szykman, J.J.; Zhang, L.; Wang, Y.X.; Chen, D. Improving the accuracy of daily satellite-derived ground-level fine aerosol concentration estimates for North America. *Environ. Sci. Technol.* **2012**, *46*, 11971–11978. [CrossRef]
22. Hersey, S.P.; Garland, R.M.; Crosbie, E.; Shingler, T.; Sorooshian, A.; Piketh, S.; Burger, R. An overview of regional and local characteristics of aerosols in South Africa using satellite, ground, and modeling data. *Atmos. Chem. Phys.* **2015**, *15*, 4259–4278. [CrossRef] [PubMed]
23. Kim, P.S.; Jacob, D.; Fisher, J.A.; Travis, K.; Yu, K.; Zhu, L.; Yantosca, R.M.; Sulprizio, M.P.; Jimenez, J.L.; Campuzano-Jost, P.; et al. Sources, seasonality, and trends of southeast US aerosol. *Atmos. Chem. Phys.* **2015**, *15*, 10411–10433. [CrossRef]
24. Torres, O.; Bhartia, P.K.; Herman, J.R.; Sinyuk, A.; Ginoux, P.; Holben, B. A Long-Term Record of Aerosol Optical Depth from TOMS Observations and Comparison to AERONET Measurements. *J. Atmos. Sci.* **2002**, *59*, 398–413. [CrossRef]

25. Xu, Y.; Bahadur, R.; Zhao, C.; Ruby Leung, L. Estimating the radiative forcing of carbonaceous aerosols over California based on satellite and ground observations. *J. Geophys. Res. Atmos.* **2013**, *118*, 11148–11160. [CrossRef]
26. Bibi, H.; Alam, K.; Chishtie, F.; Bibi, S.; Shahid, I.; Blaschke, T. Intercomparison of MODIS, MISR, OMI, and CALIPSO aerosol optical depth retrievals for four locations on the Indo-Gangetic plains and validation against AERONET data. *Atmos. Environ.* **2015**, *111*, 113–126. [CrossRef]
27. Justice, C.; Belward, A.; Morisette, J.; Lewis, P.; Privette, J.; Baret, F. Developments in the 'validation' of satellite sensor products for the study of the land surface. *Int. J. Remote Sens.* **2000**, *21*, 3383–3390. [CrossRef]
28. Loew, A.; Bell, W.; Brocca, L.; Bulgin, C.E.; Burdanowitz, J.; Calbet, X.; Donner, R.V.; Ghent, D.; Gruber, A.; Kaminski, T.; et al. Validation practices for satellite-based Earth observation data across communities. *Rev. Geophys.* **2017**, *55*, 779–817. [CrossRef]
29. Filonchyk, M.; Yan, H.; Zhang, Z.; Yang, S.; Li, W.; Li, Y. Combined use of satellite and surface observations to study aerosol optical depth in different regions of China. *Sci. Rep.* **2019**, *9*. [CrossRef]
30. Remer, L.A.; Tanré, D.; Kaufman, Y.J.; Levy, R.; Mattoo, S. Algorithm for remote sensing of tropospheric aerosol from MODIS: Collection 005. *Natl. Aeronaut. Space Adm.* **2006**, *1490*, 1–88.
31. Levy, R.C.; Remer, L.A.; Mattoo, S.A.; Vermote, E.F.; Kaufman, Y.J. Second-generation operational algorithm: Retrieval of aerosol properties over land from inversion of Moderate Resolution Imaging Spectroradiometer spectral reflectance. *J. Geophys. Res. Atmos.* **2007**, *112*. [CrossRef]
32. Kumar, N.; Chu, A.D.; Foster, A.D.; Peters, T.; Willis, R. Satellite remote sensing for developing time and space resolved estimates of ambient particulate in Cleveland, OH. *Aerosol Sci. Technol.* **2011**, *45*, 1090–1108. [CrossRef] [PubMed]
33. Bréon, F.M.; Vermeulen, A.; Descloitres, J. An evaluation of satellite aerosol products against sunphotometer measurements. *Remote Sens. Environ.* **2011**, *115*, 3102–3111. [CrossRef]
34. Mishchenko, M.I.; Liu, L.; Geogdzhayev, I.V.; Travis, L.D.; Cairns, B.; Lacis, A.A. Toward unified satellite climatology of aerosol properties. 3. MODIS versus MISR versus AERONET. *J. Quant. Spectrosc. Radiat. Transf.* **2010**, *111*, 540–552. [CrossRef]
35. Saide, P.E.; Kim, J.; Song, C.H.; Choi, M.; Cheng, Y.; Carmichael, G.R. Assimilation of next generation geostationary aerosol optical depth retrievals to improve air quality simulations. *Geophys. Res. Lett.* **2014**, *41*, 9188–9196. [CrossRef]
36. Vijayakumar, K.; Devara, P.C.; Rao, S.V.B.; Jayasankar, C.K. Dust aerosol characterization and transport features based on combined ground-based, satellite and model-simulated data. *Aeolian Res.* **2016**, *21*, 75–85. [CrossRef]
37. Drury, E.; Jacob, D.J.; Spurr, R.J.; Wang, J.; Shinozuka, Y.; Anderson, B.E.; Clarke, A.D.; Dibb, J.; McNaughton, C.; Weber, R. Synthesis of satellite (MODIS), aircraft (ICARTT), and surface (IMPROVE, EPA-AQS, AERONET) aerosol observations over eastern North America to improve MODIS aerosol retrievals and constrain surface aerosol concentrations and sources. *J. Geophys. Res. Atmos.* **2010**, *115*. [CrossRef]
38. Lei, H.; Wang, J.X.L. Observed characteristics of dust storm events over the western United States using meteorological, satellite, and air quality measurements. *Atmos. Chem. Phys.* **2014**, *14*, 7847–7857. [CrossRef]
39. Li, J.; Carlson, B.E.; Lacis, A.A. How well do satellite AOD observations represent the spatial and temporal variability of PM2.5 concentration for the United States? *Atmos. Environ.* **2015**, *102*, 260–273. [CrossRef]
40. Roy, B.; Mathur, R.; Gilliland, A.B.; Howard, S.C. A comparison of CMAQ-based aerosol properties with IMPROVE, MODIS, and AERONET data. *J. Geophys. Res. Atmos.* **2007**, *112*. [CrossRef]
41. Raman, A.; Arellano, A.F.; Sorooshian, A. Decreasing aerosol loading in the north American monsoon region. *Atmosphere* **2016**, *7*, 24. [CrossRef] [PubMed]
42. Clay, K.; Muller, N.Z. *Recent Increases in Air Pollution: Evidence and Implications for Mortality*; Technical Report; National Bureau of Economic Research: Cambridge, MA, USA, 2019. [CrossRef]
43. US EPA. *National Air Quality: Status and Trends of Key Air Pollutants | US EPA*; US EPA: Washington, DC, USA, 2019.
44. Bryson, R.A.; Hare, F.K. *Climates of North America: Volume 11 of World Survey of Climatology*; Elsevier: Amsterdam, The Netherlands, 1974.
45. Holben, B.N.; Eck, T.F.; Slutsker, I.; Tanré, D.; Buis, J.P.; Setzer, A.; Vermote, E.; Reagan, J.A.; Kaufman, Y.J.; Nakajima, T.; et al. AERONET—A federated instrument network and data archive for aerosol characterization. *Remote Sens. Environ.* **1998**, *66*, 1–16. [CrossRef]
46. Rainwater, M.; Gregory, L. *Cimel Sunphotometer (CSPHOT) Handbook*; Technical Report; Citeseer: Princeton, NJ, USA, 2005.
47. Mishra, A.K.; Rudich, Y.; Koren, I. Spatial boundaries of Aerosol Robotic Network observations over the Mediterranean basin. *Geophys. Res. Lett.* **2016**, *43*, 2259–2266. [CrossRef]
48. Shi, Y.; Zhang, J.; Reid, S.; Holben, B.; Hyer, J.; Curtis, C. An analysis of the collection 5 MODIS over-ocean aerosol optical depth product for its implication in aerosol assimilation. *Atmos. Chem. Phys.* **2011**, *11*, 557–565. [CrossRef]
49. Yang, J.; Hu, M. Filling the missing data gaps of daily MODIS AOD using spatiotemporal interpolation. *Sci. Total Environ.* **2018**, *633*, 677–683. [CrossRef] [PubMed]
50. Sayer, A.M.; Munchak, L.A.; Hsu, N.C.; Levy, R.C.; Bettenhausen, C.; Jeong, M.J.J. Modis collection 6 aerosol products: Comparison between aqua's e-deep blue, dark target, and "merged" data sets, and usage recommendations. *J. Geophys. Res.* **2014**, *119*, 13965–13989. [CrossRef]
51. Levy, R.C.; Mattoo, S.; Munchak, L.A.; Remer, L.A.; Sayer, A.M.; Patadia, F.; Hsu, N.C. The Collection 6 MODIS aerosol products over land and ocean. *Atmos. Meas. Tech.* **2013**, *6*, 2989–3034. [CrossRef]

52. Hsu, N.C.; Tsay, S.C.; King, M.D.; Herman, J.R. Aerosol properties over bright-reflecting source regions. *IEEE Trans. Geosci. Remote Sens.* **2004**, *42*, 557–569. [CrossRef]
53. Hsu, N.C.; Tsay, S.C.; King, M.; Herman, J. Deep Blue Retrievals of Asian Aerosol Properties During ACE-Asia. *IEEE Trans. Geosci. Remote Sens.* **2006**, *44*, 3180–3195. [CrossRef]
54. Hsu, N.C.; Jeong, M.J.; Bettenhausen, C.; Sayer, A.M.; Hansell, R.; Seftor, C.S.; Huang, J.; Tsay, S.C. Enhanced Deep Blue aerosol retrieval algorithm: The second generation. *J. Geophys. Res. Atmos.* **2013**, *118*, 9296–9315. [CrossRef]
55. Hsu, N.C. *Changes to Modis Deep Blue Aerosol Products betwwen Collection 6 and Collection 6.1*; NASA GSFC: Greenbelt, MD, USA, 2017.
56. Wei, J.; Li, Z.; Peng, Y.; Sun, L. MODIS Collection 6.1 aerosol optical depth products over land and ocean: Validation and comparison. *Atmos. Environ.* **2019**, *201*, 428–440. [CrossRef]
57. Ginoux, P.; Garbuzov, D.; Hsu, N.C. Identification of anthropogenic and natural dust sources using Moderate Resolution Imaging Spectroradiometer (MODIS) Deep Blue level 2 data. *J. Geophys. Res.* **2010**, *115*, D05204. [CrossRef]
58. Petrenko, M.; Ichoku, C.; Leptoukh, G. Multi-sensor aerosol products sampling system (MAPSS). *Atmos. Meas. Tech.* **2012**, *5*, 913–926. [CrossRef]
59. Eck, T.F.; Holben, B.N.; Reid, J.S.; Dubovik, O.; Smirnov, A.; O'Neill, N.T.; Slutsker, I.; Kinne, S. Wavelength dependence of the optical depth of biomass burning, urban, and desert dust aerosols. *J. Geophys. Res. Atmos.* **1999**, *104*, 31333–31349. [CrossRef]
60. Hamonou, E.; Chazette, P.; Balis, D.; Dulac, F.; Schneider, X.; Galani, E.; Ancellet, G.; Papayannis, A. Characterization of the vertical structure of Saharan dust export to the Mediterranean basin. *J. Geophys. Res. Atmos.* **1999**, *104*, 22257–22270. [CrossRef]
61. Loría-Salazar, S.M.; Holmes, H.A.; Patrick Arnott, W.; Barnard, J.C.; Moosmüller, H. Evaluation of MODIS columnar aerosol retrievals using AERONET in semi-arid Nevada and California, U.S.A., during the summer of 2012. *Atmos. Environ.* **2016**, *144*, 345–360. [CrossRef]
62. Gupta, P.; Remer, L.A.; Patadia, F.; Levy, R.C.; Christopher, S.A. High-resolution gridded level 3 aerosol optical depth data from modis. *Remote Sens.* **2020**, *12*, 2847. [CrossRef]
63. Drury, E.; Jacob, D.J.; Wang, J.; Spurr, R.J.; Chance, K. Improved algorithm for MODIS satellite retrievals of aerosol optical depths over western North America. *J. Geophys. Res. Atmos.* **2008**, *113*, 16204. [CrossRef]
64. Shi, H.; Xiao, Z.; Zhan, X.; Ma, H.; Tian, X. Evaluation of MODIS and two reanalysis aerosol optical depth products over AERONET sites. *Atmos. Res.* **2019**, *220*, 75–80. [CrossRef]